ACS OMEGA

http://pubs.acs.org/journal/acsodf

Article

Three-Dimensional Structure and Optimization of the Metallo-β-Lactamase Inhibitor Aspergillomarasmine A

Kalinka Koteva, David Sychantha, Caitlyn M. Rotondo, Christian Hobson, James F. Britten, and Gerard D. Wright*

Cite This: *ACS Omega* 2022, 7, 4170–4184

Read Online

ACCESS | Metrics & More | Article Recommendations | Supporting Information

ABSTRACT: The aminopolycarboxylic acid aspergillomarasmine A (AMA) is a natural Zn^{2+} metallophore and inhibitor of metallo-β-lactamases (MBLs) which reverses β-lactam resistance. The first crystal structure of an AMA coordination complex is reported and reveals a pentadentate ligand with distorted octahedral geometry. We report the solid-phase synthesis of 23 novel analogs of AMA involving structural diversification of each subunit (L-Asp, L-APA1, and L-APA2). Inhibitory activity was evaluated in vitro using five strains of *Escherichia coli* producing globally prevalent MBLs. Further in vitro assessment was performed with purified recombinant enzymes and intracellular accumulation studies. Highly constrained structure−activity relationships were demonstrated, but three analogs revealed favorable characteristics where either Zn^{2+} affinity or the binding mode to MBLs were improved. This study identifies compounds that can further be developed to produce more potent and broader-spectrum MBL inhibitors with improved pharmacodynamic/pharmacokinetic properties.

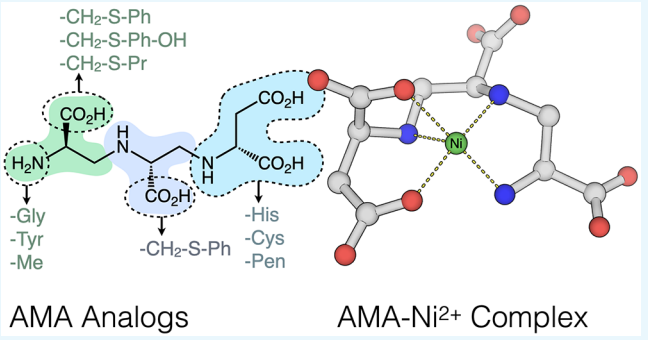

INTRODUCTION

Over 80 years ago, the discovery of β-lactam antibiotics revolutionized modern medicine with their ability to reduce the burden of infectious diseases caused by bacteria. However, the effectiveness of these life-saving drugs is diminishing due to the growing number of β-lactam-resistant bacteria.[1,2] The most common cause of resistance involves the production of β-lactamases, enzymes that eliminate antibiotic activity by catalyzing ring-opening hydrolysis of the β-lactam pharmacophore. Serine-β-lactamases (SBLs) and metallo-β-lactamases (MBLs) represent the two major groups of these enzymes and are distinguished by different catalytic mechanisms. While both result in the same inactive hydrolytic products, SBLs employ a serine nucleophile while MBLs utilize a hydroxide ion bridged by Zn^{2+} co-factors to attack the β-lactam bond (Figure 1).[3]

To safeguard existing β-lactam antibiotics from resistance, chemical strategies to inhibit β-lactamases have shown remarkable clinical impact. Six β-lactamase inhibitors (clavulanate, sulbactam, tazobactam, avibactam, vaborbactam, and relebactam) are approved for clinical use and are co-formulated with a β-lactam antibiotic in combination therapies. Several other combinations are in late-stage clinical development.[4] Although these drug combinations are effective, their spectrum of activity is limited to SBL-producing bacteria. This fact leaves the growing clinical challenge of MBLs unmet, indicating the need for MBL-targeted therapeutics.[5−10]

Over the past decades, many MBL inhibitors have been discovered.[11−15] These MBL inhibitors can be grouped into several classes based on their mechanisms of inactivation: Zn^{2+} binding inhibitors, covalent inhibitors, transition-state analogs, and allosteric inhibitors (Figure 2).[12,16] Recently discovered cyclic boronate inhibitors QPX7728 and tanirobactam (VNRX-5133) are the most promising inhibitors to date. They have been shown to inhibit SBL and MBL by mimicking the tetrahedral intermediate resulting from β-lactam ring hydrolysis. Tanirobactam has entered clinical development in combination with cefepime against carbapenem-resistant Enterobacteriaceae (CRE), carbapenem-resistant *P. aeruginosa* (CRPA), and NDM and VIM classes of MBL.[17,18] Additionally, QPX7728 has been shown have better activity against the IMP class of MBL.[19] Despite this advancement, the search for broad-spectrum inhibitors of MBLs must continue since one has yet to be approved for clinical use. In 2014, we identified a fungal Zn^{2+} metallophore, aspergillomarasmine A[20] (AMA) (Figure 2), as an inhibitor of MBLs with excellent efficacy toward NDM and VIM-type enzymes. The mechanism of action of AMA involves

Received: October 14, 2021
Accepted: December 27, 2021
Published: January 26, 2022

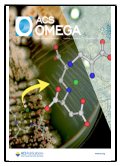

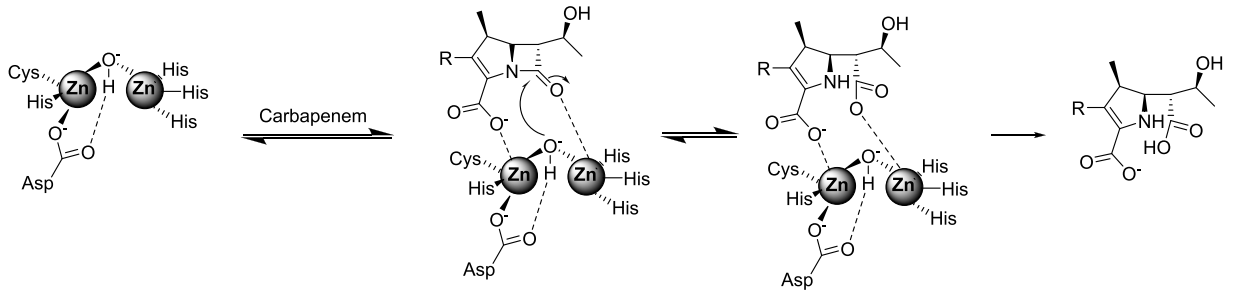

Figure 1. General mechanism of inactivation of carbapenem antibiotics by metallo-β-lactamases.

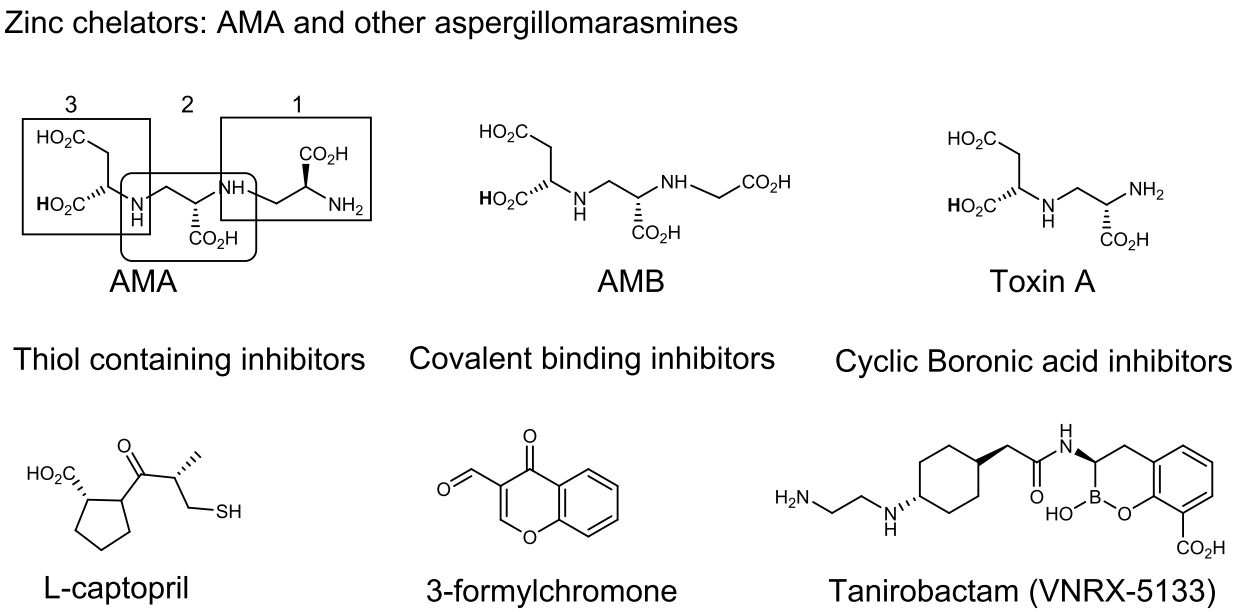

Figure 2. MBL inhibitors. Classes include zinc chelators (AMA and analogs), L-captopril as a member of zinc-binding inhibitors, 3-formylchromone as a representative of covalent binding inhibitors, and cyclic boronate inhibitor tanirobactam, closely mimicking β-lactams.

selective Zn^{2+} binding with picomolar affinity, which sequesters the metal in complex fluids.[21] Consequently, AMA indirectly inhibits MBLs by outcompeting them for Zn^{2+} even in the presence of common metals (Mg^{2+}, Ca^{2+}, and Fe^{3+}). AMA also promotes Zn^{2+} dissociation from active sites of MBLs, which accelerates the degradation of certain types of MBLs (e.g., NDM-1) in bacteria.[21] As a result, AMA restores the activity of β-lactams such as meropenem against MBL producing carbapenem-resistant bacteria in mouse models of infection while being well tolerated in the host (LD_{50} > 150 mg/kg i.v. in mice).[22]

AMA's biological activity, narrow metal-binding profile (Zn^{2+}, Ni^{2+}, and Co^{2+}), and unique chemical structure have inspired several research groups to develop methods for its total synthesis, including reductive amination,[23,24] aziridine,[25] and sulfamidate[26] approaches. Furthermore, a chemoenzymatic strategy utilizing ethylenediamine-*N*,*N*′-disuccinic acid (EDDS) lyase and the authentic AMA synthase for the synthesis of AMA was also recently reported.[27,28] However, the structural basis for metal coordination is still unknown, hindering reliable structure−activity relationship studies and optimization of potency.

In this study, we report the first crystal structure of an AMA-Ni^{2+} complex. An improved, practical route to AMA and AMA analogs via aziridine ring-opening on solid support (Scheme 1) enabled us to prepare a series of AMA derivatives carrying substitutions at all three parts of the molecule (APA1, APA2, and Asp) (Scheme 2) (Scheme 3). All the AMA analogs synthesized using these methods were studied using both in vitro antimicrobial susceptibility tests and in vitro enzyme assays against the most prevalent MBLs, including NDM-1, VIM-1, VIM-2, IMP-1, IMP-7, and IMP-27.[29,30] The selected substitutions validated the crystal structure of the AMA-Ni^{2+} complex, and structure−activity relationship (SAR) studies identified compounds with improved Zn^{2+} affinity and targeted activity as direct MBL inhibitors.

RESULTS AND DISCUSSION

Crystal Structure of AMA in Complex with Ni^{2+}. To guide the synthesis of AMA analogs and explore SAR, we aimed to determine the crystal structure of AMA in complex with a suitable metal ligand. We found that complexes of AMA with either Zn^2 or Co^{2+} were recalcitrant to crystallization, but crystals of the Ni^{2+} complex could be grown in a solution of tetramethylammonium hydroxide. X-ray diffraction analysis revealed that the asymmetric unit is composed of a single AMA-Ni^{2+} complex. The stereochemistries of the Asp, APA1, and APA2 subunits are in the *LLL* configuration as anticipated.[25] All the nitrogen atoms and carboxylate groups of the subunits are present in their protonated and deprotonated forms, respectively. Additionally, five water molecules, a sodium ion, and a tetramethylammonium ion are packed within the asymmetric

https://doi.org/10.1021/acsomega.1c05757
ACS Omega 2022, 7, 4170−4184

Scheme 1. Synthesis of APA2 AMA analogs 1−3[a]

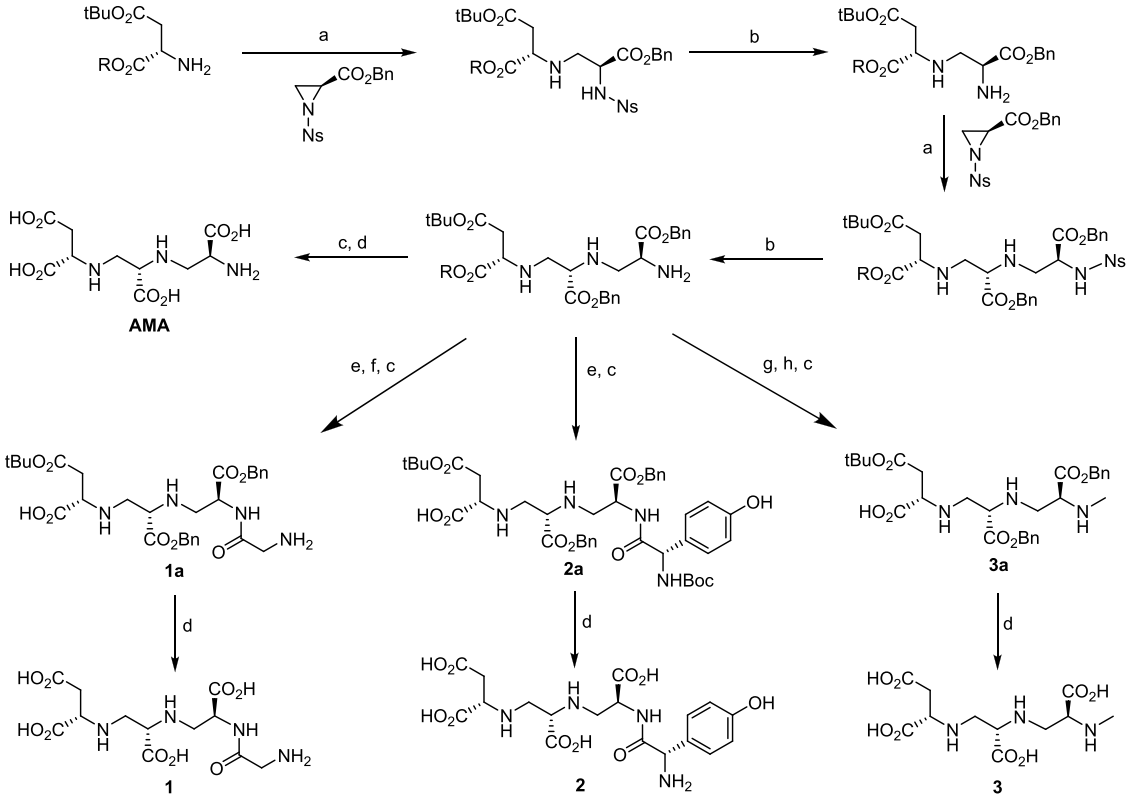

[a]Reagents and conditions: (a) *o*-Ns-L-Azy-OBn, THF, 20 h, RT; (b) PhSH, DIPEA, CH_3CN, 1 h, RT; (c) Fmoc-Gly-OH/Boc-Tyr-OH, HOBt, HBTU, DMF, 20 h, RT; (d) piperidine, DMF, 20 min, RT; (e) AcOH, TFE, DCM, 1 h, RT; (f) MeI, piperidine, DCM, 1 h, RT; (g) TFMSA, anisole, DCM, 1 h, RT. R = 2-chlorotritylchloride resin. All resin-bound intermediates were subjected to small-scale cleavage and confirmed by LC−MS.

unit and form important crystal contacts between adjacent AMA complexes (Figure 3a,b and Figure S1).

The structure reveals that AMA is a pentadentate ligand coordinated to a distorted octahedral Ni^{2+} center. Coordination occurs through AMA's three main nitrogen atoms (N2, N6, and N9) and two oxygen atoms of the Asp subunit (O4A and O1B). The sixth and final coordination site is occupied by a carboxylate oxygen (O7A) of an adjacently packed AMA-Ni^{2+} complex, which we believe is a crystallization artifact. This hypothesis is based on our previous data, which showed that the binding of either Ni^{2+} or Zn^{2+} to AMA occurs with 1:1 stoichiometry in solution.[21] Consequently, we suspect that the sixth coordination site of the AMA complex is likely occupied by solvent when dissolved under aqueous conditions. The mean Ni−L bond distances in $Ni(AMA)^{2-}$ for Ni−N and Ni−O are in the range of 2.057−2.119 (Å, and the values are comparable with corresponding bond lengths in related Ni(II) complexes (Ni−N range, 2.05−2.12 Å and Ni−O range, 2.01−2.11 Å) (Table S1).

AMA has picomolar affinity for Zn^{2+}, allowing passive inhibition of MBLs by outcompeting the enzyme for metal.[31] While such affinity is sufficient for MBL inhibition, it is weak enough to remain non-antimicrobial effects and is relatively nontoxic. The pentadentate nature of the AMA ligand provides a molecular basis of such affinity and differs from the predicted structure, which was modeled as a hexadentate complex.[32] Structurally related metal chelators that form hexadentate complexes (EDDS and EDTA) bind Zn^{2+} with subpicomolar affinity have broader metal affinity and are toxic at low concentrations. Therefore, our next aim was to use this structural information to guide the design of AMA analogs for SAR studies to inhibit MBLs by actively targeting enzyme-bound Zn^{2+} ions.

Synthesis of AMA Analogs. AMA's potency as an inhibitor is affected by both the Zn^{2+} binding strength of the competing MBL and the concentration of free Zn^{2+} present in the environment. This established the scope for developing AMA analogs that could act directly on the enzyme to overcome the current barriers associated with the sequestration mechanism.[31]

To efficiently synthesize structurally diverse analogs, we developed a solid-phase approach by modifying a well-established aziridine-based route to AMA in solution.[25] We envisioned that using a solid phase strategy[33−36] would facilitate the time-efficient preparation of a broader range of analogs in higher yield and purity (Scheme 1) (Table S2). First, we diversified the AMA scaffold by modifying the N-terminal L-diaminopropionic acid unit (APA2, Figure 2) to afford analogs **1−3** (Scheme 1). Commercially available 2-chlorotritylchloride resin preloaded with L-Asp(OtBu) was treated with *N*-nosyl-protected aziridine benzyl ester to install the first L-diaminopropionic acid unit of AMA (APA1, Figure 2). Nosyl deprotection using previously reported conditions[25,26] followed by a second ring-opening reaction furnished the *N*-nosyl protected N-terminal L-diaminopropionic acid unit (APA2). Following a further nosyl deprotection, the N-terminal amine was acylated with either Fmoc-Gly-OH or Boc-Tyr-OH using standard coupling conditions.[37,38] Removal of the Fmoc-protecting group followed by acid-catalyzed cleavage from the

https://doi.org/10.1021/acsomega.1c05757
ACS Omega 2022, 7, 4170−4184

Scheme 2. Synthesis of Thioether AMA analogs 4−9 (APA2 and APA1)[a]

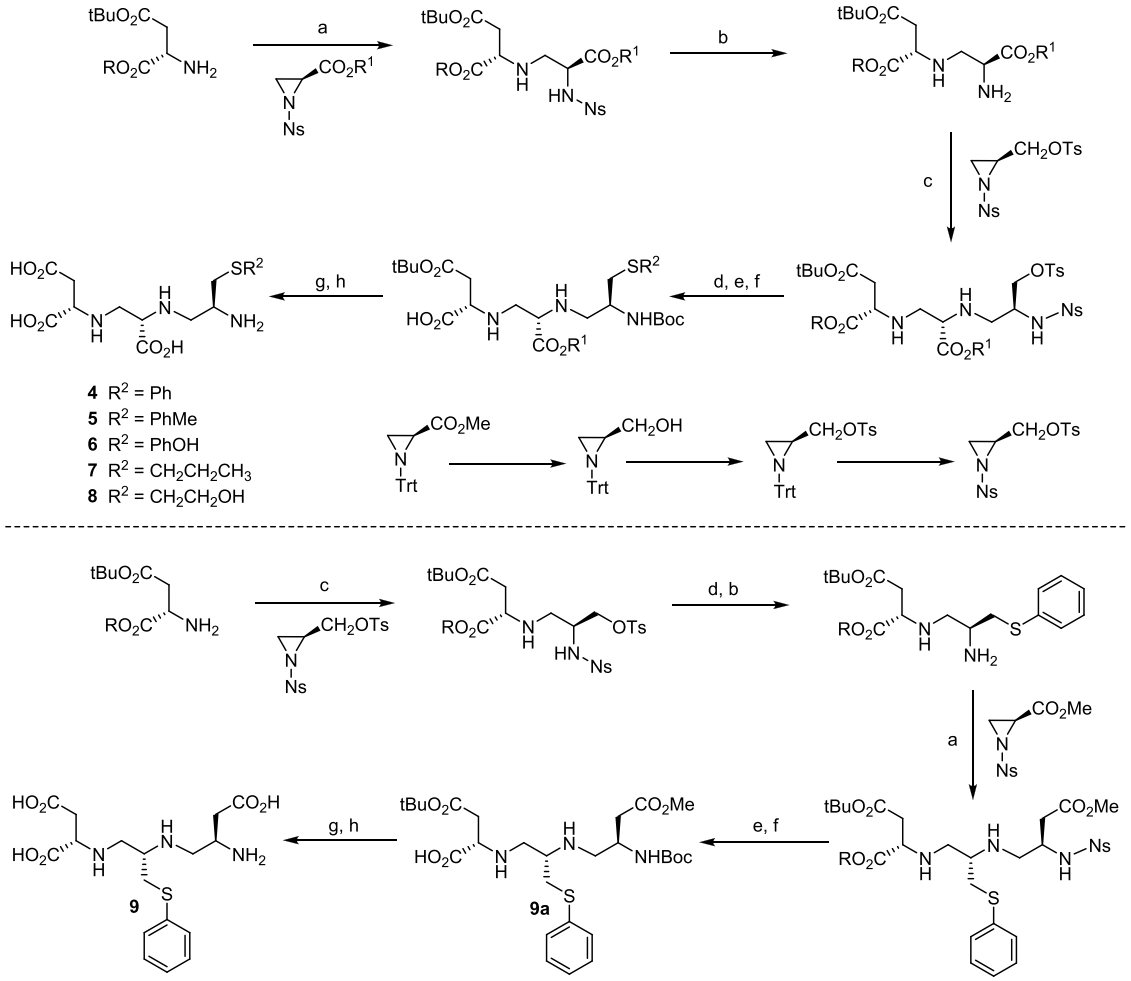

[a]Reagents and conditions: (a) *o*-Ns-L-Azy-OR,[1] THF, 20 h, RT; (b) PhSH, DIPEA, CH_3CN, 1 h, RT; (c) *o*-Ns-L-Azy-CH_2OTs, THF, 20 h, RT; (d) R^2SH, DIPEA, CH_3CN, 1 h, RT; (e) Boc_2O, DIPEA, DCM, 2 h, RT; (f) AcOH, TFE, DCM, 1 h, RT; (g) TMTOH, DCE, 4 h, 84 °C, 1 h; (h) TFMSA, anisole, DCM, 1 h, RT. R = 2-chlorotritylchloride resin, R^1 = Bn/tBu/Me. All resin-bound intermediates were subjected to small-scale cleavage and confirmed by LC−MS. *o*-Ns-L-Azy-CH_2OTs were synthesized from *o*-Trt-L-Azy-CO_2Me via previously reported procedures.[43]

resin[39] afforded protected AMA analogs **1a** and **2a**. Global deprotection using TFMSA/anisole[26] gave glycine-AMA analog **1** and tyrosine-AMA analog **2**. Using the same synthetic approach, six additional amide-substituted AMA analogs (**24**−**29**) were prepared (Table S3). To synthesize N-methylated AMA analog **3**, the *N*-nosyl protected, resin-bound AMA intermediate was N-methylated[40] before nosyl removal and cleavage from the resin afforded N-methylated intermediate **3a**. The same global deprotection conditions were used to produce N-methylated AMA analog **3**.

Since AMA's C-7 and C-10 carboxylate groups are not involved in coordinating a metal ion, we also modified these functional groups to explore their potential. Thioether substituents were chosen at these positions as there are examples in the literature of thioethers with improved biological activities.[41,42] To generate C-10 derivatives, we modified the cascade used for the synthesis of analogs **1**−**3** by using (*S*)-(1-((2-nitrophenyl) sulfonyl) aziridin-2-yl) methyl 4-methylbenzenesulfonate (Scheme 2) as the alkylating agent in the second ring-opening step.[43] The tosyl-oxy group of the resulting resin-bound intermediate could then be smoothly displaced by treatment with the appropriate thiol nucleophiles before cleavage from the resin. Global deprotection afforded the corresponding thioether analogs **4**−**8**. Similarly, C-7-derivatized thioether **9** was prepared by using (*S*)-(1-((2-nitrophenyl) sulfonyl) aziridin-2-yl) methyl 4-methylbenzenesulfonate as the alkylating reagent in the first ring-opening reaction (Scheme 2). Low-molecular weight analogs (**7** and **9**), while stable when protected, were very unstable once deprotected, resulting in anhydro products. Our attempt to displace the tosyl-oxy group with *β*-mercaptoethanol or other reactive dithiols resulted in the formation of dehydration products after global deprotection.

Finally, for the syntheses of Asp-substituted AMA analogs (**10**−**23**), we used 2-chlorotritylchloride or Wang resin preloaded with the appropriately protected amino acid[39] (Scheme 3). The same ring-opening/deprotection cascade described for analogs **1**−**3** was employed to assemble the AMA scaffold before the terminal *o*-*N*-nosyl group was substituted with an N-*t*-Boc-protecting group prior to cleavage from the resin to facilitate the final deprotection step. It is worth noting that in the case of AMA-L-Cys analog **11**, the global deprotection conditions were not sufficient to remove one or both benzyl-protecting groups. In light of this observation, we modified the syntheses of the thiol-containing AMA analogs by using *N*-nosyl aziridine methyl ester as the alkylating reagent and introducing one more deprotection step.[44]

https://doi.org/10.1021/acsomega.1c05757
ACS Omega 2022, 7, 4170−4184

Scheme 3. Synthesis of Asp-substituted AMA analogs 10−23[a]

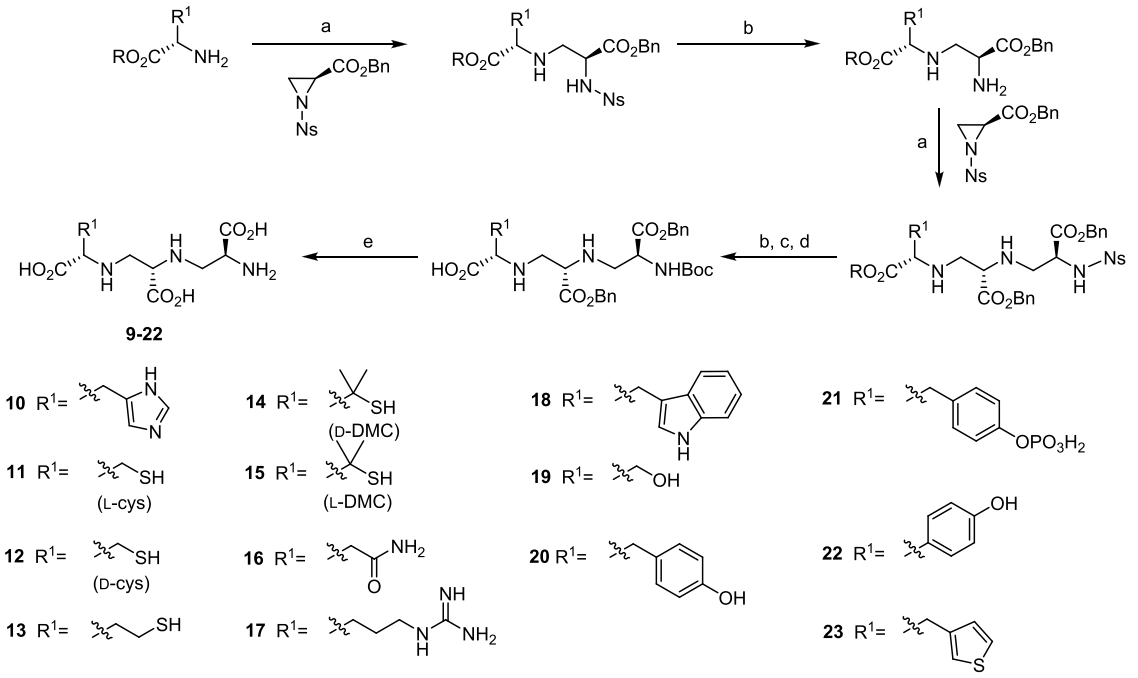

[a]Reagents and conditions: (a) *o*-Ns-L-Azy-OR,[2] THF, 20 h, RT; b) PhSH, DIPEA, CH_3CN, 1 h, RT; c) Boc_2O, DIPEA, DCM, 2 h, RT; d) AcOH, TFE, DCM, 1 h, RT; e) TFMSA, anisole, DCM, 1 h, RT; f) TMTOH, DCE, 4 h, 84 °C, 1 h; g) *o*-Ns-L-Azy-CH_2OTs, THF, 20 h, RT; h) TFA, DCM, 1 h, RT. R = 2-chlorotritylchloride resin or Wang resin. R^2 = Bn/tBu/Me, DMC (dimethyl cysteine or penicillamine (Pen). All resin-bound intermediates were subjected to small-scale cleavage and confirmed by LC−MS.

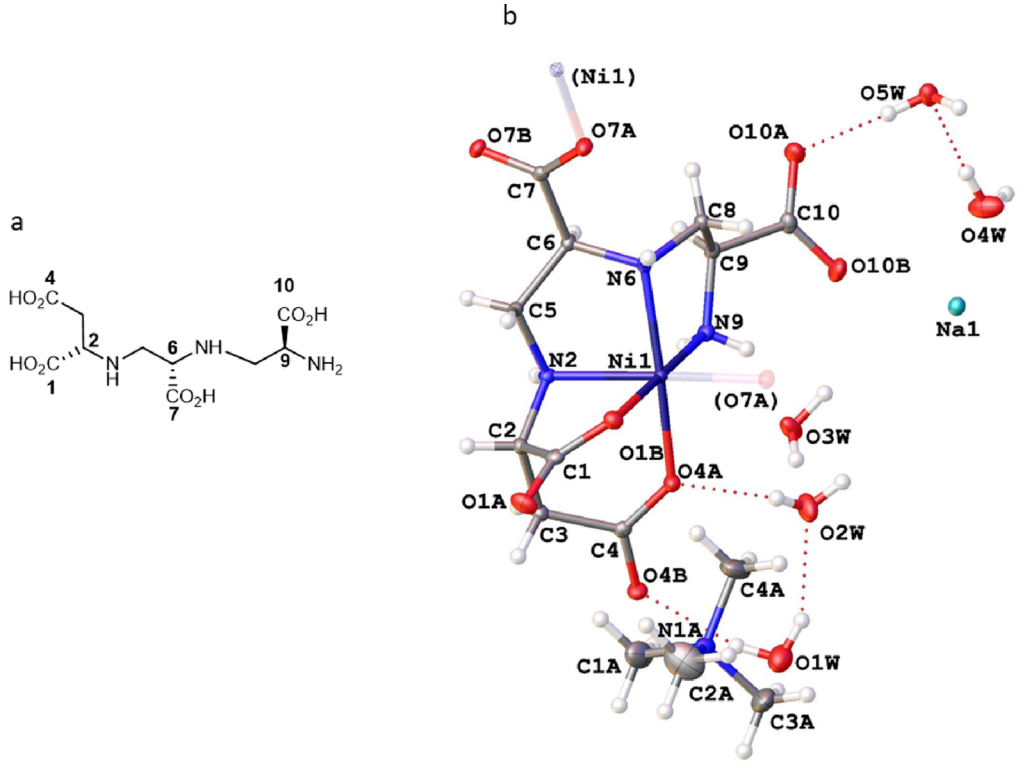

Figure 3. Crystals of AMA-Ni complex- $C_{14}H_{35}N_4NaNiO_{13}$. (a) Structure of AMA with AMA with numbered atoms involved in the Ni complex formation. (b) In the AMA-Ni complex, the coordination occurs through AMA's three main nitrogen atoms (N2, N6, and N9) and two oxygen atoms of the Asp subunit (O4A and O1B). The sixth and final coordination site is occupied by a carboxylate oxygen (O7A) of an adjacently packed AMA-Ni^{2+} complex, which is a crystallization artifact.

All final products were characterized by ^{1}H NMR, ^{13}C NMR, and high-resolution mass spectrometry (HRMS). High-performance liquid chromatography for UV-active compounds confirmed >95% purity (Supporting Information).

https://doi.org/10.1021/acsomega.1c05757
ACS Omega 2022, 7, 4170−4184

Table 1. In Vitro and Cell-Based Activities of AMA Analogs (1−9), Bearing Substitution at APA1 and APA2[e]

compound	$K_{d,Zn2}$ (nM)	IC_{50} (μM)[a]				RC (μg/mL) in MHB[b,c]				
		NDM-1 - Zn	NDM-1 + Zn	VIM-2 - Zn	IMP-7 - Zn	NDM-1	VIM-1	VIM-2	IMP-7	IMP-27
AMA	0.1 ± 0.02	12,800 ± 722	13 ± 0.2	3000	53,000	8	8	8	32	32
1	19.9 ± 3.2	>500	>100	-[d]	-	>64	-	-	-	-
2	1.4 ± 0.56	>500	>100	-	-	>64	-	-	-	-
3	8.7 ± 0.9	>500	95.3 ± 3	-	-	64	-	-	-	-
4	0.40 ± 0.07	150 ± 16	12.5 ± 0.8	246 ± 23	32 ± 3.1	8	8	4	32	64
5	1.4 ± 0.56	97.2 ± 34.2	104 ± 2.0	-	-	32	32	32	>64	>64
6	7.8 ± 3.4	>500	54 ± 4.1	183 ± 10	>500	8	4	8	16−32	32
7	109.0 ± 40	>500	29.2 ± 1	-	-	>64	-	-	-	-
8	60.0 ± 13.0	>500	>250	-	-	64	32	32	>64	>64
9	2.3 ± 1.9	>500	58 ± 5	-	-	>64	-	-	-	-

[a]In vitro assay. [b]Rescue concentration was determined at the susceptibility breakpoint of meropenem (2 μg/mL). [c]Increases in rescue concentration values are highlighted as follows: ≤ 2 increases bolded. [d]Hyphens represent values not determined, as the RC against *ndm-1*-containing *E. coli* is ≥64 μg/mL. [e]RC, rescue concentration; MHB Mueller−Hinton Broth.

Table 2. In Vitro and Cell-Based Activities of AMA Analogs (10−23), Bearing Substitution at the C-Terminal Aspartic Acid[e,f]

compound	$K_{d,Zn2}$ (nM)	IC_{50} (μM)[a]				RC (μg/mL) in MHB[b,c]				
		NDM-1 - Zn	NDM-1 + Zn	VIM-2 - Zn	IMP-7 - Zn	NDM-1	VIM-1	VIM-2	IMP-7	IMP-27
AMA	0.1 ± 0.02	12,800 ± 722	13 ± 0.2	3000	53,000	8	8	8	32	32
10	<0.0003	173.3 ± 3.9	21.7 ± 3.9	136 ± 5	>500	8	8	8	16	16
11	0.2 ± 0.05	21.5 ± 0.8	15.6 ± 0.2	22 ± 1	328 ± 15	32	32	16	>64	>64
12	4.4 ± 1.8	5.8 ± 0.5	403.8 ± 18.2	-[d]	-	32	>64	>64	>64	>64
13	-	>1000	>100	-	-	64	>64	64	>64	>64
14	2.6 ± 0.4	184.6 ± 7.8	112.4 ± 4.8	246 ± 17	>500	32	64	16	32	>64
15[e]	2.3 ± 0.4	98.6 ± 4.0	56.1 ± 2.5	361 ± 29	>500	32	16	8	16	32
16	1.0 ± 0.1	>1000	18.3 ± 0.7	-	-	16	16	16	>64	>64
17	24 ± 6	>1000	>100	-	-	>64	>64	64	>64	>64
18	18.0 ± 11.1	>1000	>100	-	-	>64	>64	>64	>64	>64
19	4.5 ± 1.75	>1000	80 ± 0.7	-	-	32	32	16	>64	>64
20	0.64 ± 0.17	172 ± 1.5	38 ± 1.8	-	-	16	16	8	>64	>64
21	10.8 ± 8.1	25.1 ± 8.3	54.0 ± 5.6	-	-	64	>64	64	>64	>64
22	9.5 ± 6.5	23 ± 3.6	283 ± 27.4	-	-	>64	>64	64	>64	>64
23	4.2 ± 2.5	9.7 ± 1.7	42.2 ± 4.1	-	-	64	32	16	>64	>64

[a]In vitro assay. [b]Rescue concentration was determined at the susceptibility breakpoint of meropenem (2 μg/mL). [c]Increases in rescue concentration values are highlighted as follows: ≤ 2 increases bolded. [d]Hyphens represent values not determined, as the RC against *ndm-1*-containing *E. coli* is ≥64 μg/mL. [e]MIC of 64 μg/mL. [f]RC, rescue concentration; MHB Mueller−Hinton Broth.

Characterization of AMA Analogs. A total of 29 AMA analogs (Table S2, Table S3) were synthesized, and their activities were evaluated based on three criteria: biological activity, in vitro MBL inhibition, and Zn^{2+} affinity. The biological activity of each compound was assessed by determining the concentration of compound necessary to restore the antibacterial activity of meropenem (2 μg/mL) against resistant *E. coli* (MIC 64 μg/mL) and is reported as the rescue concentration (RC).[45] The RC is 8 μg/mL for AMA purified from fermentation broth. The in vitro enzyme inhibition assays were performed to distinguish between direct and indirect inhibition of MBLs. This distinction was established by examining dose-dependent inhibition using two different buffer conditions: Zn^{2+}-supplemented (10 μM) or Zn^{2+}-depleted (Chelex-100-treated). Compounds **1−9** (Table 1) and **24−29** (data not shown) were first tested for biological activity against *E. coli* expressing bla_{NDM-1} and purified recombinant NDM-1. Compounds that exhibited satisfactory performance were further tested against *E. coli* producing bla_{VIM-1}, bla_{VIM-2}, bla_{IMP-7}, and bla_{IMP-27} as well as recombinant VIM-2 and IMP-7. For compounds **10−23** (Table 2), the susceptibility of all the aforementioned *E. coli* strains was assessed in parallel, and recombinant NDM-1 was initially tested in vitro. The most potent compounds were further tested with recombinant VIM-2 and IMP-7 in vitro.

The rationale for using two conditions in our in vitro enzyme inhibition assays is based on our previous work on NDM-1 inhibition. It was shown that AMA sequesters Zn^{2+} and indirectly inactivates NDM-1 in a time-dependent manner, where the rate-limiting step is the spontaneous dissociation of Zn^{2+} from the enzyme.[21] The mechanism could be described by a one-step kinetic scheme independent of AMA concentration because only free Zn^{2+} ions are acted on directly. Therefore, inhibition is strongly influenced by the concentration of Zn^{2+} in the assay buffer. This explains why the IC_{50} value of AMA toward NDM-1 is similar to the Zn^{2+} concentration in the assay buffer (IC_{50} 13 μM, when $[Zn^{2+}]$ is 10 μM) and why the corresponding dose−response curve is very steep (Hill coefficient ≈ 4).[22] However, a different effect arises when the amount of AMA is suitably high (>1 mM) as the inhibition rate becomes concentration-dependent, indicating that under these conditions, inhibition occurs in two steps, which likely involves the direct removal of Zn^{2+} by a short-lived collision complex. We further examined this phenomenon using an in vitro dose−

https://doi.org/10.1021/acsomega.1c05757
ACS Omega 2022, 7, 4170−4184

response assay with NDM-1 and determined that the Zn^{2+}-independent IC_{50} value of AMA is 12 mM. Therefore, distinguishing Zn^{2+} chelation versus direct Zn^{2+}-removal (i.e., enzyme binding) can be accomplished by comparing NDM-1 inactivation in buffers containing or lacking Zn^{2+}. Such detail is necessary to deconvolute mixed modes of inhibition.

SAR of APA1 and APA2: Modifications at C-10 (4−8) and C-7 (9). Modifying the metal coordinating amine (N9) of L-APA2 through *N*-acylation with Gly (compound **1**), Tyr (compound **2**), or compounds **24−29** (Table S2, data not shown) or N-methylation (compound **3**) considerably reduced the biological activity of AMA (RC > 64 μg/mL) (Table 1). Our in vitro dose−response inhibition assays were consistent with these observations and showed that these compounds did not inhibit recombinant NDM-1 either, which was reflected in their reduced Zn^{2+} affinity. Therefore, the N9 atom of AMA is not amenable to modification, validating its importance as a metal coordination site.

Modifying the C-10 position of L-APA2, which does not participate in metal coordination, with different hydrophobic thioether-linked substituents (compounds **4−8**) (Table 1) produced mixed effects. Aliphatic substituents (compounds **7** and **8**) had inadequate biological activities similar to the previous series of compounds. In contrast, phenyl and 4-hydroxyphenyl substituents (compounds **4** and **6**) had satisfactory biological activities comparable to AMA (bla_{NDM-1} RC 8 μg/mL). Our in vitro dose−response inhibition assays showed that compounds **4** and **6** could inactivate MBLs indirectly and that compound **4** had notable activity as a direct inhibitor of NDM-1. These observations were similar in experiments involving MBLs of the VIM and IMP groups. Conversely, 4-tolyl modification (compound **5**) abrogated biological activity despite having reasonable in vitro potency as both a direct and indirect inhibitor. These data generally indicate that the phenyl group at the C-10 position of compound **4** significantly improves MBL interactions in vitro; however, structural variations at the *para* position can significantly modify such behavior and/or reduce biological efficacy. The context-dependence of the activity of these analogs suggests that there are additional factors beyond MBL inhibition that affect efficacy and could involve complex mechanisms of action. For example, ligand field stabilization energy (LFSE) arises from an incompletely filled d orbital. Zn^{2+} has a filled d^{10} electronic orbital and has zero LFSE where the cost of breaking octahedral symmetry is relatively low, showing high rates of ligand dissociation. Therefore, substitutions near metal-ligands could affect affinity by further increasing the rate of dissociation for the ligand, explaining why some of the substitutions have led to reduced Zn^{2+} affinity and biological activity.

Nevertheless, we were encouraged by the characteristics of the phenyl group of compound **4** and thus installed a thioether-linked phenyl group at the C-7 position of L-APA1 (compound **9**) (Table 1). In contrast to our prior observations, the phenyl substituent of compound **9** did not promote direct inhibition of NDM-1. It was inactive in biological assays despite being active as an indirect inhibitor of NDM-1 in vitro. These data further support the hypothesis that the biological activity of these analogs is multifactorial and complex, requiring deeper investigation to elucidate their mechanisms.

SAR of L-Asp (10−23). Metal coordination by the sidechain of the L-Asp subunit provided an opportunity to generate diverse analogs through substitutions with different natural and unnatural amino acids (Table 2).

We initially focused on hydrophobic and/or cyclic substitutions to potentially improve enzyme binding (compounds **10**, **18**, and **20−23**). Except for compound **10**, phenyl-based analogs (compounds **20−22**) and most heterocyclic substitutions (compounds **18** and **23**) had impaired biological activity (RC > 8 μg/mL) despite exhibiting favorable activity within in vitro enzyme assays where both direct and indirect inhibition was observed. These contextual activities were similar to some of the compounds from the previous series, which further highlights the involvement of additional factors in the efficacy of AMA analogs. The exception, compound **10**, which has an L-Asp → L-His substitution, had slightly improved biological and in vitro activities relative to AMA, having the ability to bind Zn^{2+} with higher affinity. The Zn^{2+} affinity of compound **10** could not be precisely determined because it was outside the detection range of our assay, but it was estimated to be subpicomolar or lower. In light of these observations, additional nitrogen-containing side chains involving substitutions L-Asn and L-Arg (compounds **16** and **17**) were produced. Still, they did not exhibit the same positive effects, suggesting that their side chains do not possess the correct geometry and/or ionization potential for Zn^{2+} binding.

We next screened various cysteine-based analogs because thiols are known to intercalate between the Zn^{2+} cofactors of MBLs and have been successfully applied in other inhibitor design campaigns. Therefore, we generated several L-Cys and D-Cys-based analogs (compounds **11−15**) (Table 2) but found that thiol incorporation negatively affected potency in biological assays despite exhibiting both direct and indirect enzyme inhibition for some enzymes in vitro. In this case, we suspect that the limited biological activity is influenced by the oxidation state of the thiol groups of these compounds. Evidence for the oxidation of thiol-based MBL inhibitions has been previously reported and shown to be time-dependent in culture media, which negatively correlates with MBL inhibition. Of this group of compounds, antimicrobial activity (MIC = 64 μg/mL) was uniquely observed for compound **15** in the absence of meropenem. Compound **15** is the L-isomer of compound **14**, which has antimicrobial activity, and it possesses an L-Asp → L-β,β-dimethylCys substitution. Therefore, we speculate that it may be targeting an essential metalloprotein(s) in *E. coli*.

Next, we evaluated the efficacy of selected AMA analogs with promising in cell activities against two other Gram-negative bacterial pathogens: *Klebsiella pneumoniae*- and *Acinetobacter baumannii*-expressing NDM-1 (Table 3). The results confirmed that analogs **4**, **10**, and **15** show activity comparable to AMA in combination with meropenem in *K. pneumoniae*. Surprisingly, compound **15** rescues the meropenem activity at a lower concentration than AMA when tested against *A. baumannii*. Additionally, this L-penicillamine-containing analog also showed antimicrobial activity of 32 μg/mL and 16 μg/mL for *Klebsiella* and *Acinetobacter* strains, respectively.

Intracellular Accumulation Studies. To reconcile context-specific activities among the AMA analogs, we investigated their potential to accumulate within bacterial cells.[46,47] This was achieved by incubating the compounds (50 μM) with wild-type *E. coli* cells that did not possess a bla_{MBL} gene and comparing their accumulation to meropenem and AMA, which served as references (MEM = 43.9 nmol/10^{12} CFU; AMA = 5.7 nmol/10^{12} CFU) (Figure 4 and Tables S4 and S5). We hypothesized that compounds that exhibit acceptable activity (RC ≤16 μg/mL) in biological assays might accumulate within the bacteria to a greater extent than those with low activity (RC ≥32 μg/mL).

https://doi.org/10.1021/acsomega.1c05757
ACS Omega 2022, 7, 4170−4184

Table 3. Meropenem Rescue Activities of AMA Analogs against *K. pneumoniae* ATCC 33495::pGDP2 (NDM-1) and *A. baumannii* ATCC 17978 pROTO2: NDM-1[d]

	RC (μg/mL) in MHB[a,b]	
compound	*K. pneumoniae* ATCC 33495::pGDP2 (NDM-1)	*A. baumannii* ATCC 17978::pROTO2 (NDM-1)
AMA	8	4–8
4	8	8
6	16	8
10	8	4–8
15[c]	8	2–4
16	32	16
20	64	32

[a]Rescue concentration was determined at the susceptibility breakpoint of meropenem (2 μg/mL). [b]Meropenem MIC = 16–32 μg/mL. [c]MIC = 16–32 μg/mL. [d]RC, rescue concentration.

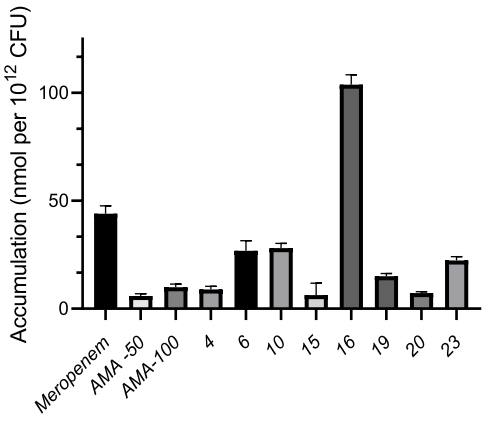

Figure 4. Cell accumulation assay data for selected analogs in *E. coli* BW25113 (WT). All assays were performed in biological and technical triplicates. The error bars represent the standard deviations.

In the cases of compounds **4** and **6**, which demonstrated the most potent activity among the L-APA2 series of analogs, intracellular accumulation increased 1.5- and 4.5-fold relative to AMA, respectively. In contrast, the remaining compounds of this series, which had insufficient biological activity, could not be detected within the intracellular contents of *E. coli* and were therefore unable to penetrate the cells. Similar results were observed for the compounds of the L-Asp series of analogs. While the accumulation of compounds with acceptable activities (compounds **10**, **15**, **16**, **19**, **20**, and **23**) increased, those with insufficient activity could not be detected.

Several physiochemical properties predict the likelihood of a small molecule to accumulate within Gram-negative bacteria, including the presence and position of a primary amine, globularity, and flexibility (number of rotatable bonds). As AMA can exist either in free or metal-coordinated forms, predictive rules may not accurately inform the accumulation of analogs as their physiochemical properties are dynamic. This was implied from the varied accumulation of AMA analogs with similar globularity and flexibility (e.g., AMA vs compound **10**). Alternative phenomena potentially responsible for the varied accumulation of AMA analogs are localized polarity and steric effects near the amine, which could be directly influenced by metal coordination but cannot be assessed without structural data for each analog.[48] Overall, these data validated our hypothesis that the SAR of these analogs is linked to intracellular concentration. Furthermore, the data suggest that improved intracellular accumulation can be leveraged to enable analogs with weaker Zn^{2+} affinity (relative AMA), such as compounds **6**, **14**, **15**, **16**, and **23**, to exert a reasonable extent of inhibitory activity.

CONCLUSIONS

In summary, we report the crystal structure of AMA in complex with Ni^{2+} and identified the key functional groups involved in metal coordination. The structure was used to guide the design of AMA analogs, which were generated using a new and efficient total solid-phase synthesis strategy with 2-chlorotritylchloride resin. Antimicrobial susceptibility assays and in vitro enzyme inhibition assays were performed and involved representative members of the three most prevalent groups MBLs (NDM, VIM, and IMP). Moreover, Zn^{2+} affinity and intracellular accumulation were assessed for a subset of the most active compounds to establish a comprehensive structure–activity relationship profile.

Of the modifications to the C-10 atom of APA1, aliphatic substitutions were not tolerated. In contrast, aromatic phenyl and hydroxyphenyl substitutions either performed similarly to AMA or lowered/raised the RC of some MBLs 2-fold, whereas a methylated derivative had a negative impact. These findings indicate that a polar carboxyl group at C-10 is not essential for activity and that moderately hydrophobic and polar aromatic groups are well tolerated, showing potential for further expansion.

The substitution of L-Asp with alternative amino acids was not tolerated in most cases as analogs with polar, hydrophobic, or thiol side chains had reduced efficacy, underscoring the importance of metal coordination geometry of this residue. The one exception, which contained an L-Asp → L-His substitution, showed 2-fold reductions in RC toward *E. coli*, producing MBLs with high tolerance to AMA. This finding indicates that the side chain of L-His improves Zn^{2+} coordination, which increases its affinity and enables it to outcompete MBLs with higher Zn^{2+} affinity, which are usually are more recalcitrant to AMA.

While the inhibitory mechanism of AMA only involves indirect Zn^{2+} sequestration, some analogs could facilitate both indirect and direct removal of Zn^{2+} from the active sites of MBLs; however, the biological potency of such analogs did not surpass AMA. It stands to reason that in a Zn^{2+}-rich environment, such as culture media, inhibition by sequestration is thermodynamically more favorable than direct Zn^{2+} removal through a collision complex. Therefore, a poorer chelator is less likely to be an efficient MBL inhibitor despite accumulating within the cell and transiently removing Zn^{2+} from the enzyme through direct attack. In this case, the inactive MBL could reactivate by binding Zn^{2+} not sequestered by the chelator. This contrasts with a stronger chelator, which may result in off-target activity by outcompeting host metalloproteins. In conclusion, our SAR studies highlight that intracellular Zn^{2+} sequestration dynamics are crucial for biological activity, indicating that metal affinity and local concentration likely play the most important roles in MBL inhibition.

EXPERIMENTAL SECTION

Preparation of AMA-Ni Complex- $(CH_3)_4$N-Ni-AMA $(H_2O)_5$. Single crystals of $C_{14}H_{35}N_4NaNiO_{13}$ [AMA-Ni] were prepared following the protocol published for the EDDA-Ni complex.[49] Briefly, AMA (46 mg, 0.14 mmol, 1 eq), $NiCO_3 \cdot H_2O$

https://doi.org/10.1021/acsomega.1c05757
ACS Omega 2022, 7, 4170–4184

(45 mg, 0.14 mmol, 1 eq), and tetramethylammonium hydroxide pentahydrate (51 mg, 0.28 mmol, as 10% aqueous solution, 2 eq) were stirred in water (0.6 mL). The resulting blue-violet solution was heated to 65 °C (steam water bath) for 1 h with stirring. After that time, the solution was filtered while hot, and crystals were grown by slow evaporation.

Single-Crystal Diffraction Experiment of the AMA-Ni Complex. A suitable crystal was selected and mounted on a Bruker APEX-II CCD diffractometer. The crystal was kept at 100.0(1) K during data collection. Using Olex2,[50] the structure was solved with the XT[51] structure solution program using Intrinsic Phasing and refined with the XL[52] refinement package using Least Squares minimization. Crystal data for $C_{14}H_{35}N_4NaNiO_{13}$ (M = 549.16 g/mol): monoclinic, space group $P2_1$ (no. 4), a = 9.4899(4) Å, b = 10.0977(4) Å, c = 12.5037(5) Å, β = 97.280(2)°, V = 1188.52(8) Å^3, Z = 2, T = 100.0(1) K, μ(Mo K_α) = 0.904 mm^{-1}, $Dcalc$ = 1.535 g/cm^3, 47,260 reflections measured (3.284° ≤ 2Θ ≤ 61°), 7265 unique (R_{int} = 0.0349, R_{sigma} = 0.0315) which were used in all calculations. The final R_1 was 0.0236 (I > 2σ(I)) and wR_2 was 0.0542 (all data). Full structural details are available from the CCDC (deposition number 2105011). Additional crystallographic details could be found in Table S1.

Synthesis of AMA Analogs. All compounds are >95% pure by HPLC analysis (Supporting Information).

*((S)-2-(((S)-2-(2-Aminoacetamido)-2-carboxyethyl)-amino)-2-carboxyethyl)-L-aspartic Acid (**1**).* The preloaded 2-chlorotrityl resin was left to swell by suspending 1 g in 10 mL of anhydrous DMF for 30 min at RT before removing the solvent by filtration. A 20% v/v solution of piperidine in DMF (10 mL) was then added, followed by shaking for 20 min at RT. The resin was then filtered and washed with DMF (3 × 10 mL), IPA (3 × 10 mL), DMF (1 × 10 mL), and THF (2 × 10 mL). To the resin-bound amino acid was added a solution of *o*-Ns-Azy-OBn (3 eq) in THF (5 mL) under N_2, and the system was sealed. The ring-opening reaction was then carried out for 20 h at RT with shaking. The remaining resin-bound Ns-protected intermediate was treated with acetonitrile (5 mL), followed by thiophenol (1 mL) and DiPEA (1 mL). The reaction was incubated with shaking for 1 h at RT. The resulting resin was washed with DMF/IPA/THF as described above, and to it was added a fresh solution of *o*-Ns-Azi-OBn (3 eq in 5 mL of THF). The second ring-opening reaction was carried out as described above. The Nosyl group of the resin-bound, fully protected AMA was removed using PhSH/DIPEA as already described. The resin was then filtered and washed with DMF/IPA and treated with Fmoc-Gly-OH (5 eq), HOBt (5 eq), and HBTU (5 eq) in DMF (10 mL/g resin) for 20 h at RT with shaking.[37] Then, the resin was filtered and washed with DCM/MeOH before treatment with piperidine (20%) in DMF to remove the Fmoc group. Cleavage from the resin as described above afforded the protected glycine-AMA analog **1a**, which was then treated with TFMSA (9 eq) and anisole (10 eq) in DCM for 1 h at RT[26] to remove the acid-protecting groups to yield glycine-AMA analog **1**; ^{1}H NMR (700 MHz, D_2O) δ 5.06 (dd, J = 13.3, 4.5 Hz, 1H), 4.56 (s, 2H), 4.28 (dd, J = 10.9, 5.0 Hz, 1H), 3.92 (dd, J = 11.1, 4.5 Hz, 1H), 3.66−3.60 (m, 1H), 3.58 (dd, J = 7.0, 3.8 Hz, 1H), 2.96 (dd, J = 13.2, 11.0 Hz, 1H), 2.82−2.67 (m, 4H). ^{13}C NMR (176 MHz, D_2O) δ 182.38, 179.45, 175.37, 172.08, 169.85, 57.91, 56.58, 55.67, 44.50, 41.86, 39.71, 24.22.

*((S)-2-(((S)-2-((R)-2-Amino-3-(4-hydroxyphenyl)-propanamido)-2-carboxyethyl)amino)-2-carboxyethyl)-L-aspartic Acid (**2**).* The tyrosine-AMA analog **2** was synthesized using a similar procedure to that described for the synthesis of glycine-AMA analog **1** using Boc-Tyr-OH (5 eq). The Boc group was removed during the final deprotection step with TFMSA/anisole as described above to afford tyrosine-AMA analog **2**; ^{1}H NMR (700 MHz, D_2O) δ 7.22 (q, J = 6.8 Hz, 3H), 6.94−6.89 (m, 3H), 4.43 (d, J = 8.9 Hz, 1H), 4.34 (t, J = 7.2 Hz, 1H), 4.01 (d, J = 7.0 Hz, 1H), 3.92 (d, J = 6.0 Hz, 2H), 3.54 (d, J = 7.1 Hz, 2H), 3.51−3.41 (m, 1H), 3.35−3.22 (m, 1H), 3.22−3.10 (m, 0H), 2.98−2.70 (m, 2H). ^{13}C NMR (176 MHz, D_2O) δ 172.81, 169.58, 155.15, 130.90, 125.49, 122.32, 120.52, 118.71, 116.91, 115.93, 59.87, 54.51, 52.22, 35.80, 35.22.

*((S)-2-Carboxy-2-(((S)-2-carboxy-2-(methylamino)ethyl)-amino) Ethyl)-L-aspartic Acid (**3**).* *N*-Methylation was carried out as previously described[40] using fully protected, resin-bound AMA. Methylation was followed by nosyl deprotection via treatment with mercaptoethanol (10 eq) and DBU (5 eq) in *N*-methyl pyrrolidone (5 mL) for 5 min at RT. The procedure was then repeated to ensure full deprotection before the N-methylated product was cleaved from the resin as described above to afford **3a.** The acid-protecting groups of **3a** were removed using TFMSA/anisole as described above to afford fully deprotected N-methylated AMA analog **3**; ^{1}H NMR (700 MHz, D_2O) δ 4.58 (dd, J = 13.6, 5.4 Hz, 1H), 4.49 (dd, J = 10.7, 5.3 Hz, 1H), 4.18 (dd, J = 8.8, 5.4 Hz, 1H), 3.78−3.66 (m, 2H), 3.31 (td, J = 14.8, 13.4, 10.8 Hz, 1H), 3.16−3.06 (m, 1H), 2.94 (s, 3H), 2.75−2.67 (m, 2H), 2.07 (d, J = 1.0 Hz, 1H).^{13}C NMR (176 MHz, D_2O) δ 177.94, 177.15, 174.78, 167.65, 62.12, 56.11, 55.20, 43.04, 42.05, 37.85, 33.60.

General Procedure for the Synthesis of Thioether AMA Analogs 4−8. After the first ring-opening reaction and nosyl deprotection as described above, the resulting resin was washed with DMF/IPA/THF as described above, and to it was added a fresh solution of *o*-Ns-Azy-CH_2OTs[43] (3 eq in 5 mL of THF). The second ring-opening reaction was carried out as described above. Small-scale cleavage and LC−MS analysis confirmed that the second ring-opening had gone to completion to afford fully protected, resin-bound tosyl-AMA. Then to the resin was added acetonitrile (5 mL/g resin) followed by the corresponding thiol (1 mL) and DIPEA (1 mL). After 1 h shaking at RT, the corresponding thioether was formed and the nosyl group was removed in most cases, except for propane thiol and *p*-methylbenzene thiol **5** where the Ns group had to be additionally deprotected. The resin-bound AMA analog was then Boc-protected using Boc_2O (5 eq) and DIPEA (10 eq) in DCM[53] to yield a fully protected resin-bound thioether. Cleavage from the resin followed by deprotection using TFMSA/anisole as described above where R^1 = Bn/tBu, or using TMTOH in DCM at 84 °C for 3 h where R^1 = Me, afforded analogs **4−8**.

*(S)-2-(((S)-2-Amino-3-(phenylthio)propyl)amino)-2-carboxyethyl)-L-aspartic Acid (**4**).* ^{1}H NMR (700 MHz, D_2O) δ 7.58−7.51 (m, 2H), 7.44 (dd, J = 8.4, 7.0 Hz, 2H), 7.41−7.33 (m, 1H), 3.81 (dd, J = 9.3, 3.7 Hz, 1H), 3.44−3.37 (m, 1H), 3.37−3.31 (m, 2H), 3.28 (dd, J = 12.9, 4.2 Hz, 1H), 3.21 (dd, J = 14.7, 8.0 Hz, 1H), 3.13 (dd, J = 12.9, 9.8 Hz, 1H), 3.04 (dd, J = 13.8, 6.9 Hz, 1H), 2.81 (ddd, J = 15.4, 3.7, 1.8 Hz, 2H), 2.69 (dd, J = 17.6, 9.3 Hz, 1H). ^{13}C NMR (176 MHz, D_2O) δ 177.31, 177.14, 172.98, 132.88, 130.78, 129.57, 127.73, 97.86, 67.45, 64.24, 59.79, 59.27, 50.43, 47.88, 47.38, 35.63, 33.89, 23.67.

*((S)-2-(((S)-2-Amino-3-(P-tolylthio)propyl)amino)-2-carboxyethyl)-L-aspartic Acid (**5**).* ^{1}H NMR (700 MHz, D_2O) δ 7.53−7.38 (m, 2H), 7.33−7.19 (m, 3H), 3.77 (dd, J = 9.3, 3.8 Hz, 0H), 3.63−3.42 (m, 1H), 3.39−3.30 (m, 1H), 3.30−3.22

https://doi.org/10.1021/acsomega.1c05757
ACS Omega 2022, 7, 4170−4184

(m, 1H), 3.19 (dd, J = 14.5, 5.6 Hz, 0H), 3.16−3.10 (m, 1H), 3.10−3.03 (m, 1H), 2.99 (ddd, J = 13.6, 5.5, 2.8 Hz, 1H), 2.83−2.74 (m, 1H), 2.69−2.58 (m, 1H), 2.34 (dd, J = 7.0, 3.6 Hz, 4H).^{13}C NMR (176 MHz, D_2O) δ 179.11, 177.63, 177.47, 171.02, 138.29, 131.39, 131.21, 130.21, 60.27, 59.40, 54.11, 50.29, 48.96, 47.91, 36.02, 32.78, 28.41, 23.27, 20.10.

*((S)-2-(((S)-2-Amino-3-((4-hydroxyphenyl)thio)propyl)-amino)-2-carboxyethyl)-L-aspartic Acid (**6**).* ^{1}H NMR (700 MHz, D_2O) δ 7.52−7.39 (m, 3H), 6.91 (dq, J = 8.5, 2.0, 1.6 Hz, 3H), 3.90 (ddd, J = 9.0, 3.6, 0.7 Hz, 1H), 3.85−3.70 (m, 2H), 3.35 (dp, J = 8.6, 4.6 Hz, 1H), 3.30 (d, J = 4.8 Hz, 1H), 3.28−3.21 (m, 1H), 3.14−3.02 (m, 2H), 2.98 (dd, J = 13.7, 7.1 Hz, 1H), 2.85−2.75 (m, 3H), 2.73 (s, 1H), 2.71−2.63 (m, 2H), 1.92 (s, 1H). ^{13}C NMR (176 MHz, D_2O) δ 177.55, 177.23, 174.27, 171.02, 160.25, 134.59, 122.30, 120.50, 118.70, 116.73, 59.96, 59.39, 52.24, 50.30, 47.92, 38.70, 36.59, 23.24.

*((S)-2-(((S)-2-Amino-3-(propylthio)propyl)amino)-2-carboxyethyl)-L-aspartic Acid (**7**).* ^{1}H NMR (700 MHz, D_2O) δ 3.85 (dd, J = 7.0, 4.1 Hz, 1H), 3.75 (dd, J = 6.5, 4.0 Hz, 1H), 3.52−3.42 (m, 1H), 3.24 (dd, J = 13.5, 4.1 Hz, 1H), 3.10−3.03 (m, 2H), 2.95−2.87 (m, 1H), 2.87−2.80 (m, 2H), 2.80−2.71 (m, 3H), 2.65−2.55 (m, 3H), 1.62 (dq, J = 10.3, 3.5, 3.0 Hz, 2H), 0.97 (tt, J = 7.4, 1.2 Hz, 4H). ^{13}C NMR (176 MHz, D_2O) δ 180.61, 180.15, 177.76, 60.52, 58.31, 50.91, 49.72, 47.22, 38.69, 33.66, 31.48, 22.14, 12.51.

*((S)-2-(((S)-2-Amino-3-((2-hydroxyethyl)thio)propyl)-amino)-2-carboxyethyl)-L-aspartic Acid (**8**).* ^{1}H NMR (700 MHz, D_2O) δ 3.85−3.71 (m, 1H), 3.71−3.63 (m, 1H), 3.61−3.46 (m, 1H), 3.46−3.34 (m, 1H), 3.35−3.20 (m, 1H), 3.20−3.03 (m, 1H), 3.02−2.89 (m, 1H), 2.86−2.65 (m, 2H), 2.65−2.53 (m, 1H). ^{13}C NMR (176 MHz, D_2O) δ 177.29, 172.95, 171.64, 120.52, 118.71, 60.53, 60.22, 60.01, 53.30, 51.19, 46.84, 44.16, 36.49, 35.51, 34.47, 34.06.

*((S)-2-(((S)-2-Amino-2-carboxyethyl)amino)-3-(phenylthio)propyl)-L-aspartic Acid (**9**).* The order of the two ring-opening steps used for the synthesis of analogs **4**−**8** was exchanged to produce analog **9**, where the thioether was incorporated after the first ring-opening reaction. ^{1}H NMR (700 MHz, D_2O) δ 7.58−7.51 (m, 2H), 7.43 (dd, J = 8.4, 7.0 Hz, 2H), 7.39−7.32 (m, 1H), 3.76 (dd, J = 5.3, 3.9 Hz, 1H), 3.67 (dd, J = 9.8, 3.6 Hz, 1H), 3.37−3.29 (m, 1H), 3.27−3.20 (m, 2H), 3.06−2.98 (m, 2H), 2.95 (td, J = 13.4, 12.8, 9.0 Hz, 1H), 2.81 (dd, J = 13.3, 4.0 Hz, 1H), 2.78−2.67 (m, 2H), 2.64−2.55 (m, 1H). ^{13}C NMR (176 MHz, D_2O) δ 177.70, 177.65, 173.69, 133.94, 130.77, 129.52, 127.43, 59.43, 54.42, 53.71, 48.58, 45.98, 38.70, 36.59, 35.02.

General Procedures and Spectral Data for Asp-Substituted AMA Analogs 10−23. Asp-substituted AMA analogs **10**−**23** were synthesized using the same ring-opening/deprotection cascade described above, starting from the appropriate protected amino acid-substituted resin (trityl- or Pbf-protected). TFMSA/anisole was used for the final deprotection where R^2 = Bn/tBu, and TMTOH was used where R^2 = Me. Final deprotection conditions also resulted in the removal of the trityl/Pbf amino acid-protecting groups. The 2-chlorotrityl resin was used to synthesize all analogs, except for the His-substituted analog **10** where Wang resin was used.

*(S)-2-Amino-3-(((S)-1-carboxy-2-(((S)-1-carboxy-2-(1H-imidazol-4-yl)ethyl)amino)ethyl)amino)propanoic Acid (**10**).* His-substituted AMA analog **10** was synthesized according to the above general procedure using Trt-D-His-substituted Wang resin. Once the chain had been assembled, TFA:DCM (95: 5) was used to cleave the analog from the resin, followed by TFMSA/anisole deprotection described above, which also resulted in trityl deprotection, to afford His-substituted AMA analog **10**. ^{1}H NMR (700 MHz, D_2O) δ 7.85−7.81 (m, 1H), 7.09 (d, J = 10.5 Hz, 1H), 3.90 (dd, J = 7.0, 5.6 Hz, 1H), 3.81 (dd, J = 6.3, 4.1 Hz, 1H), 3.36 (dd, J = 9.3, 5.0 Hz, 1H), 3.29−3.14 (m, 5H), 3.04 (ddd, J = 12.6, 9.0, 4.6 Hz, 1H), 2.94−2.87 (m, 1H). ^{13}C NMR (176 MHz, D_2O) δ 177.49, 173.62, 173.10, 136.11, 116.51, 62.23, 60.08, 54.60, 48.02, 47.04, 27.43.

*(S)-2-Amino-3-(((S)-1-carboxy-2-(((S)-1-carboxy-2-mercaptoethyl) amino)ethyl)amino)propanoic Acid (**11**).* Cys-substituted AMA analog **11** was synthesized according to the above general procedure using Trt-L-Cys-substituted resin. ^{1}H NMR (700 MHz, D_2O) δ 4.07 (dd, J = 7.7, 4.3 Hz, 1H), 3.86 (dt, J = 10.6, 5.3 Hz, 1H), 3.48−3.41 (m, 2H), 3.37 (dt, J = 12.5, 4.8 Hz, 1H), 3.31−3.22 (m, 2H), 3.16 (ddd, J = 14.1, 9.3, 5.1 Hz, 1H), 2.96 (dt, J = 13.3, 4.1 Hz, 1H). ^{13}C NMR (176 MHz, D_2O) δ 177.09, 172.91, 171.81, 60.65, 59.70, 54.50, 48.29, 46.91, 36.92.

*(S)-2-Amino-3-(((S)-1-carboxy-2-(((R)-1-carboxy-2-mercaptoethyl)amino)ethyl)amino)propanoic Acid (**12**).* D-Cys-substituted AMA analog **12** was synthesized according to the above general procedure using Trt-D-Cys-substituted resin. ^{1}H NMR (700 MHz, D_2O) δ 4.57−4.49 (m, 1H), 4.42 (t, J = 5.4 Hz, 1H), 4.32−4.27 (m, 1H), 4.23−4.13 (m, 4H), 4.05−3.95 (m, 2H), 3.82−3.73 (m, 2H), 3.67−3.56 (m, 3H), 3.30−3.19 (m, 4H), 3.17−3.11 (m, 2H). ^{13}C NMR (176 MHz, D_2O) δ 174.48, 172.15, 168.44, 167.73, 124.11, 122.31, 120.51, 118.71, 60.25, 60.08, 53.37, 49.82, 44.37, 25.89.

*((S)-2-(((S)-2-Amino-2-carboxyethyl)amino)-2-carboxyethyl)-L-homocysteine (**13**).* L-Homocysteine-substituted AMA analog **13** was synthesized according to the above general procedure using the corresponding Trt-propanethiol-substituted resin. ^{1}H NMR (700 MHz, D_2O) δ 4.72 (ddd, J = 4.6, 3.0, 1.3 Hz, 1H), 4.40 (td, J = 6.1, 1.6 Hz, 1H), 4.27 (td, J = 6.5, 1.5 Hz, 1H), 4.07 (ddd, J = 14.9, 6.2, 1.5 Hz, 1H), 4.03−3.91 (m, 2H), 3.81 (ddd, J = 13.4, 5.6, 1.6 Hz, 1H), 2.80−2.69 (m, 2H), 2.51−2.41 (m, 1H), 2.18−2.07 (m, 1H). ^{13}C NMR (176 MHz, D_2O) δ 171.07, 168.98, 166.86, 121.48, 119.68, 117.88, 116.07, 57.46, 52.84, 50.29, 47.18, 40.49, 32.05, 19.28.

*(R)-2-(((S)-2-(((S)-2-Amino-2-carboxyethyl)amino)-2-carboxyethyl)amino)-3-mercapto-3-methylbutanoic Acid (**14**).* D-DMC-substituted AMA analog **14** was synthesized according to the above general procedure using the corresponding Trt-D-DMC-substituted resin. ^{1}H NMR (700 MHz, D_2O) δ 3.89−3.77 (m, 1H), 3.50−3.43 (m, 1H), 3.37 (d, J = 3.1 Hz, 1H), 3.27 (dd, J = 13.5, 6.1 Hz, 1H), 3.14 (dd, J = 9.9, 7.2 Hz, 1H), 2.99−2.87 (m, 1H), 1.61 (d, J = 5.0 Hz, 3H), 1.34 (d, J = 8.6 Hz, 3H). ^{13}C NMR (176 MHz, D_2O) δ 177.56, 177.41, 173.07, 73.87, 59.36, 54.51, 48.90, 46.93, 44.29, 41.13, 32.84.

*(S)-2-(((S)-2-(((S)-2-Amino-2-carboxyethyl)amino)-2-carboxyethyl)amino)-3-mercapto-3-methylbutanoic Acid (**15**).* L-DMC-substituted AMA analog **15** was synthesized according to the above general procedure using the corresponding Trt-L-DMC-substituted resin. ^{1}H NMR (700 MHz, D_2O) δ 3.86 (ddd, J = 26.8, 6.3, 4.4 Hz, 1H), 3.66 (s, 0H), 3.56−3.44 (m, 1H), 3.29−3.11 (m, 3H), 3.11−2.93 (m, 1H), 1.66−1.57 (m, 5H), 1.48−1.40 (m, 4H). ^{13}C NMR (176 MHz, D_2O) δ 177.37, 177.15, 176.85, 172.83, 73.29, 69.66, 58.47, 51.12, 49.11, 44.35, 27.61, 21.92.

((S)-2-(((S)-2-Amino-2-carboxyethyl)amino)-2-carboxyethyl)-L-asparagine (16). L-Asparagine-substituted AMA analog **16** was synthesized according to the above general procedure using the corresponding Trt-L-asparagine-substituted

https://doi.org/10.1021/acsomega.1c05757
ACS Omega 2022, 7, 4170−4184

resin.^{1}H NMR (700 MHz, D_2O) δ 3.86 (dd, J = 8.0, 4.3 Hz, 1H), 3.76 (dd, J = 6.0, 4.0 Hz, 1H), 3.33 (dd, J = 9.6, 4.6 Hz, 1H), 3.26−3.20 (m, 1H), 3.18 (dd, J = 13.5, 6.0 Hz, 1H), 3.05−2.99 (m, 1H), 2.89 (dd, J = 16.9, 4.4 Hz, 1H), 2.85−2.76 (m, 2H). ^{13}C NMR (176 MHz, D_2O) δ 177.30, 174.46, 173.04, 60.08, 58.57, 58.47, 54.79, 54.59, 48.12, 47.76, 47.51, 47.04, 41.07, 33.91.

*((S)-2-(((S)-2-Amino-2-carboxyethyl)amino)-2-carboxyethyl)-L-arginine (**17**).* L-Arginine-substituted AMA analog **17** was synthesized according to the above general procedure using the corresponding Pbf-L-arginine-substituted resin ^{1}H NMR (700 MHz, D_2O) δ 3.82−3.71 (m, 1H), 3.50−3.39 (m, 1H), 3.38−3.29 (m, 1H), 3.24 (td, J = 7.6, 6.9, 1.9 Hz, 2H), 3.17 (ddd, J = 13.5, 6.6, 1.2 Hz, 1H), 3.13−3.00 (m, 1H), 2.96−2.77 (m, 2H), 1.91−1.74 (m, 1H), 1.74−1.58 (m, 2H). ^{13}C NMR (176 MHz, D_2O) δ 178.34, 177.55, 173.88, 160.25, 156.73, 120.49, 118.69, 62.43, 61.38, 58.34, 54.67, 48.45, 47.43, 40.61, 27.68, 24.21, 24.01.

*(S)-2-Amino-3-(((S)-1-carboxy-2-(((S)-1-carboxy-2-(1H-indol-2-yl)ethyl)amino)ethyl)amino)propanoic Acid (**18**).* L-Tryptophan-substituted AMA analog **18** was synthesized according to the above general procedure using L-tryptophan-substituted resin. ^{1}H NMR (700 MHz, D_2O) δ 7.77 (dq, J = 7.9, 1.0 Hz, 1H), 7.56 (dq, J = 8.3, 1.0 Hz, 1H), 7.38 (d, J = 7.1 Hz, 1H), 7.34−7.29 (m, 1H), 7.23 (ddq, J = 8.0, 7.0, 1.0 Hz, 1H), 4.01 (t, J = 6.7 Hz, 1H), 3.58−3.49 (m, 2H), 3.40−3.35 (m, 2H), 3.27 (ddd, J = 9.2, 5.3, 1.5 Hz, 1H), 3.23−3.15 (m, 1H), 3.09−3.01 (m, 2H), 2.77 (ddt, J = 13.6, 4.1, 1.1 Hz, 1H), 2.74 (t, J = 0.9 Hz, 3H), 2.09−2.07 (m, 1H), 1.93 (t, J = 0.9 Hz, 1H). ^{13}C NMR (176 MHz, D_2O) δ 122.32, 120.52, 118.72, 116.92, 112.05, 62.56, 54.73, 47.98, 46.90, 38.72.

*(S)-2-Amino-3-(((S)-1-carboxy-2-(((S)-1-carboxy-2-hydroxyethyl)amino)ethyl)amino)propanoic Acid (**19**).* L-Serine-substituted AMA analog **19** was synthesized according to the above general procedure using L-serine-substituted resin. ^{1}H NMR (700 MHz, D_2O) δ 4.10−4.04 (m, 1H), 4.02−3.94 (m, 2H), 3.90−3.76 (m, 4H), 3.46−3.42 (m, 1H), 3.42−3.36 (m, 2H), 3.32−3.22 (m, 2H), 3.13 (ddt, J = 12.3, 9.9, 1.0 Hz, 1H), 2.92 (ddt, J = 13.6, 4.1, 1.1 Hz, 1H). ^{13}C NMR (176 MHz, D_2O) δ 177.28, 172.97, 171.36, 63.43, 59.79, 59.05, 54.65, 47.80, 46.99.

*(S)-2-Amino-3-(((S)-1-carboxy-2-(((S)-1-carboxy-2-(4-hydroxyphenyl)ethyl)amino)ethyl)amino)propanoic Acid (**20**).* L-Tyrosine-substituted AMA analog **20** was synthesized according to the above general procedure using L-tyrosine-substituted resin. ^{1}H NMR (700 MHz, D_2O) δ 7.26−7.15 (m, 2H), 6.95−6.85 (m, 2H), 3.82 (tt, J = 6.6, 1.5 Hz, 1H), 3.74 (ddt, J = 6.5, 4.1, 0.9 Hz, 1H), 3.32 (ddt, J = 9.4, 5.1, 1.0 Hz, 1H), 3.25−3.08 (m, 4H), 3.04−2.93 (m, 1H), 2.87 (ddt, J = 13.5, 4.1, 0.9 Hz, 1H). ^{13}C NMR (176 MHz, D_2O) δ 177.55, 173.92, 173.14, 154.82, 130.69, 126.95, 115.80, 63.88, 59.99, 54.68, 48.19, 47.03, 35.17.

*(S)-2-Amino-3-(((S)-1-carboxy-2-(((S)-1-carboxy-2-(4-(phosphonooxy)phenyl)ethyl)amino)ethyl)amino)propanoic Acid (**21**).* L-Phosphotyrosine-substituted AMA analog **21** was synthesized according to the above general procedure using L-phosphotyrosine-substituted resin. ^{1}H NMR (700 MHz, D_2O) δ 7.32 (d, J = 8.0 Hz, 2H), 7.21 (d, J = 8.0 Hz, 2H), 4.32−4.21 (m, 1H), 4.13 (q, J = 6.8, 6.4 Hz, 1H), 3.96−3.82 (m, 1H), 3.59−3.46 (m, 2H), 3.46−3.36 (m, 2H), 3.36−3.23 (m, 2H), 2.72 (s, 1H). ^{13}C NMR (176 MHz, D_2O) δ 172.46, 170.21, 167.20, 151.64, 130.65, 129.53, 121.11, 120.50, 118.70, 59.05, 56.44, 51.06, 48.14, 41.72, 38.70, 33.92.

The starting L-Phosphotyrosine (pTyr) was not a single enantiomer. This fact is contributing to the peak splitting in the HPLC chromatogram (Supporting Information).

*(S)-2-Amino-3-(((S)-1-carboxy-2-(((S)-carboxy(4-hydroxyphenyl)methyl)amino)ethyl)amino)propanoic Acid (**22**).* *p*-Hydroxyphenylglycine-substituted AMA analog **22** was synthesized according to the above general procedure using *p*-hydroxyphenylglycine-substituted resin. ^{1}H NMR (700 MHz, D_2O) δ 7.36 (dd, J = 8.6, 3.5 Hz, 2H), 7.03−6.92 (m, 3H), 4.65 (d, J = 11.3 Hz, 1H), 3.85−3.74 (m, 1H), 3.34−3.26 (m, 1H), 3.22 (pd, J = 11.5, 6.8 Hz, 1H), 3.11−3.01 (m, 1H), 3.01−2.90 (m, 1H), 2.90−2.81 (m, 1H), 2.73 (d, J = 0.9 Hz, 2H). ^{13}C NMR (176 MHz, D_2O) δ 177.38, 173.05, 156.88, 130.49, 122.30, 120.50, 118.70, 116.90, 116.18, 65.32, 60.17, 54.63, 47.32, 47.03, 38.70, 32.99.

*(S)-2-Amino-3-(((S)-1-carboxy-2-(((S)-1-carboxy-2-(thiophen-2-yl)ethyl)amino)ethyl)amino)propanoic Acid (**23**).* Thiophene-substituted AMA analog **23** was synthesized according to the above general procedure using thiophene-substituted resin. ^{1}H NMR (700 MHz, D_2O) δ 7.35−7.26 (m, 1H), 7.02 (ddd, J = 4.8, 3.4, 1.1 Hz, 1H), 6.98−6.91 (m, 1H), 3.53−3.42 (m, 1H), 3.42−3.29 (m, 1H), 3.26−3.09 (m, 3H), 2.87−2.71 (m, 3H), 2.60 (ddd, J = 12.1, 9.0, 1.3 Hz, 1H). ^{13}C NMR (176 MHz, D_2O) δ 180.42, 180.28, 178.29, 139.84, 127.18, 126.36, 124.62, 64.96, 63.50, 55.36, 50.04, 49.68, 32.86.

Determination of Zn^{2+} Affinity. The Zn^{2+} affinities of AMA analogs were determined through Zn^{2+} competition with a colorimetric 4-(2-pyridylazo) resorcinol (PAR)-based assay as described previously for AMA (**21**). AMA analogs were titrated into Chelex-100 treated buffer (20 mM HEPES and 100 mM NaCl, pH 7.5) containing excess PAR (100 μM) and $ZnSO_4$ (10 μM). Assays were incubated in clear flat-bottom 96-well plates for 3 h at 25 °C with a final assay volume of 200 μL. Dissociation of Zn^{2+} from PAR due to competition results in a decrease in absorbance at a wavelength of 492 nm, which was measured with a BioTek Synergy H1 microplate reader. The dissociation constant for AMA was estimated using the known stability constant of PAR at pH 7.4 using the method described by Kocyla et al.[54]

Bacterial Antimicrobial Susceptibility Tests. DNA manipulations and pGDP2 plasmid construction for *E. coli and K. pneumoniae* were performed as described previously.[31] However, for *A. baumannii* plasmid construction, the *A. baumannii* origin of replication (ori1266) from pFLP2 (vector was a gift from Dr. Ayush Kumar at the University of Manitoba) was added to empty pGDP2 using restriction enzyme digestion with Psp1406I (AclI) followed by Gibson Assembly. PCR amplification of ori1266 and Gibson Assembly were carried out using the following primers: 5′ CAT GCC CGG TTA CTG GAA CGT TGA TCG TAG AAA TAT CTA TGA TTA TC 3′ and 5′ CAT ACC GCC AGT TGT TTA CCC TCA CGG ATT TTA ACA TTT TGC GTT G 3′. The *Escherichia*−*Acinetobacter* shuttle vector containing *bla*NDM-1 was obtained by restriction enzyme digestion with NcoI/XhoI and Gibson Assembly. PCR amplification of *bla*NDM-1 (from existing pGDP2:NDM-1) and Gibson Assembly were conducted using the following primers: 5′ CTT TAA GAA GGA GAT ATA CCA TGG GCA GCA GCC ATC ATC ATC ATC 3′ and 5′ GTG GTG GTG GTG GTG CTC GAG TGC GGC CGC AAG CTT 3′. All vector sequences were verified by Sanger Sequencing.

Bacterial antibiotic susceptibility tests were conducted based on previously described protocols.[31,55] Briefly, meropenem was dissolved in water while AMA was diluted in water containing

https://doi.org/10.1021/acsomega.1c05757
ACS Omega 2022, 7, 4170−4184

≤5% (v/v) ammonium hydroxide to ensure that the final pH was between 7.5−8.5. AMA analogs were dissolved in either water (compounds **2**−**23**) or a mixture of 50% methanol/50% water (compound **1**). All compounds were filter-sterilized. All assays were conducted in half of a 96-well round base microtest plate (Sarstedt, Nümbrecht, Germany) with a final assay volume of 100 μL. Five 2-fold dilutions of meropenem were added to rows A to E, while six 2-fold dilutions of AMA or analog were added to columns 1 through 6. Although varying slightly between compounds, the 2-fold dilutions of meropenem, AMA, and analogs remained in the 0.5−64 μg/mL range. The dilutions of meropenem and AMA or analog were added to rows F and G, respectively, to confirm the minimum inhibitory concentration (MIC) value of both the antibiotic and the inhibitor with the bacterial strain. The bacterial inoculum was prepared from the bacterial cells of interest using colonies picked from overnight plates whose OD_{625} was adjusted to 0.08−0.10. Once the optimal OD_{625} was reached, a 200-fold dilution of the inoculum was conducted before its addition to the MIC plate. The dilution of the inoculum was performed using Mueller−Hinton broth (MHB). The inoculum was added to each well containing the antibiotic/inhibitor combinations. The bacterial inoculum and the MHB were added alternatively to row H to serve as growth and sterility controls. After a 20 h static incubation at 37 °C, bioassay plates were shaken for 5 min to resuspend the bacterial cells. The bioassay plates were read spectrophotometrically at a wavelength of 600 nm using a BioTek Synergy H1 plate reader (Biotek, Winooski, VT). All assays were conducted with at least two replicates. The susceptibility breakpoints published by the European Committee on Antimicrobial Susceptibility Testing (EUCAST; http://eucast.org/clinical_breakpoints/) for meropenem (2 μg/mL) were used as a reference.

Enzyme Assays. Protein purification was conducted as previously described.[31] Enzyme assays were typically performed under two different conditions. In the zinc-abundant condition, the assays were conducted in buffer containing 50 mM HEPES (pH 7.5), 0.2% (v/v) DMSO, 1% (w/v) polyethylene glycol 4000 (PEG 4000), and 10 μM $ZnSO_4$. PEG 4000 was used to prevent protein adsorption. Alternatively, in the low-zinc condition, the enzyme assays were performed in a similar buffer as described above, except there was no addition of $ZnSO_4$. In addition, 5 g of Chelex 100 (Bio-Rad, Hercules, CA) was added to every 100 mL of buffer prepared. The addition of Chelex 100 ensured the removal of any zinc ions still present in the assay buffer. This ion exchange resin was incubated with the buffer for 2 h before its removal through filtration. Once the buffers were prepared, the enzyme assays were conducted in a final volume of 200 μL using either meropenem or nitrocefin as a substrate. Prior to the initiation of the assays, the enzyme was preincubated in the assay buffer for 5−10 min at room temperature. Enzyme concentrations were 4 nM for NDM-1, VIM-2, and IMP-7. During the preincubation step, varying inhibitor concentrations (AMA or analog) could be added to the assay to determine kinetics parameters such as the half-inhibitory (IC_{50}) concentration. Alternatively, the "Chelexed" assay buffer could be supplemented with different concentrations of $ZnSO_4$ during preincubation to determine kinetics parameters such as the zinc dissociation constant (K_D).

Following incubation, the assay was initiated with the addition of the substrate. Nitrocefin and meropenem were added to the assays at final concentrations of 30 and 50 μM, respectively. The assays were red in a 96-well flat bottom plate (Thermo Fisher Scientific, Rochester, NY) using a BioTek Synergy H1 plate reader. The absorbance was measured at 490 nm (nitrocefin) or 300 nm (meropenem). Enzyme assays were followed for 60 s. The kinetic parameters (IC_{50} and $K_{D,Zn}$) were determined by plotting the linear portion of the progress curves using GraphPad Prism 9 (GraphPad, La Jolla, CA). All enzyme assays were done in duplicates.

Cell Penetration Assay. Cell penetration assays were performed as previously described[31,48] using wild-type *E. coli* BW25113 cells. Briefly, AMA (50 or 100 μM) or its analogs (50 μM) were added to cells (875 μL) before incubation (10 min at 37 °C). A volume of 800 μL of the cells with the corresponding compound was then washed through ice-cold silicone oil (700 μL) (9:1 AR20/Sigma High-Temperature Oil) by centrifugation (12,000*g*, 2 min, RT). The cells were resuspended in 200 μL of water and lysed by three freeze−thaw cycles. Cell debris was collected by centrifugation (17,000*g*, 2 min, RT) using a Fisher Scientific accuSpin Micro 17 microcentrifuge (Thermo Fisher Scientific), and the pellet was extracted with 100 μL of MeOH. The cell extracts were pooled and quantitatively analyzed by ultra-performance liquid chromatography (uplc) coupled to a high-resolution quadrupole time-of-flight (Q-TOF) 6550 mass spectrometer (Agilent, Santa Clara, CA). Samples were loaded onto a C8 column (Agilent Eclipse XDB-C8; 100 mm × 2.1 mm; 3.5 μm) previously equilibrated with solvent A (water, 0.1% formic acid) and 5% solvent B (acetonitrile, 0.1% formic acid), and they were resolved using a linear gradient of 5−97% B over 7 min, followed by a 1 min wash step at 97% B at a flow rate of 0.4 mL/min. The Q-TOF was operated in extended dynamic range positive-ion targeted MS/MS modes with an *m/z* range of 100−1700 *m/z* and a capillary voltage of 0.5 kV. The collision energies and respective parent−daughter ion transitions used for each analog are listed in Table S5. Quantification was carried out with a calibration curve of each antibiotic using Agilent MassHunter Quantitative Analysis software. For each analog, biological and technical replicates were conducted in triplicate.

■ ASSOCIATED CONTENT

Supporting Information

The Supporting Information is available free of charge at https://pubs.acs.org/doi/10.1021/acsomega.1c05757.

Additional crystallographic data; full analytical details (HPLC and HRMS data); copies of ^{1}H and ^{13}C-NMR spectra (PDF)

■ AUTHOR INFORMATION

Corresponding Author

Gerard D. Wright − *David Braley Centre for Antibiotic Discovery, M.G. DeGroote Institute for Infectious Disease Research, Department of Biochemistry and Biomedical Sciences, McMaster University, Hamilton, ON L8N 3Z5, Canada*; orcid.org/0000-0002-9129-7131; Email: wrightge@mcmaster.ca

Authors

Kalinka Koteva − *David Braley Centre for Antibiotic Discovery, M.G. DeGroote Institute for Infectious Disease Research, Department of Biochemistry and Biomedical Sciences, McMaster University, Hamilton, ON L8N 3Z5, Canada*

David Sychantha − *David Braley Centre for Antibiotic Discovery, M.G. DeGroote Institute for Infectious Disease Research, Department of Biochemistry and Biomedical*

https://doi.org/10.1021/acsomega.1c05757
ACS Omega 2022, 7, 4170−4184

Sciences, McMaster University, Hamilton, ON L8N 3Z5, Canada

Caitlyn M. Rotondo − *David Braley Centre for Antibiotic Discovery, M.G. DeGroote Institute for Infectious Disease Research, Department of Biochemistry and Biomedical Sciences, McMaster University, Hamilton, ON L8N 3Z5, Canada*

Christian Hobson − *David Braley Centre for Antibiotic Discovery, M.G. DeGroote Institute for Infectious Disease Research, Department of Biochemistry and Biomedical Sciences, McMaster University, Hamilton, ON L8N 3Z5, Canada; Willow Biosciences, Burnaby, BC V5M 3Z3, Canada*

James F. Britten − *McMaster Analytical X-ray Diffraction Facility (MAX), McMaster University, Hamilton, ON L8N 3Z5, Canada*

Complete contact information is available at: https://pubs.acs.org/10.1021/acsomega.1c05757

Author Contributions

K.K. and C.H. performed the synthesis of analogs; K.K., D.S., and C.M.R. performed the biological analyses; K.K set up the crystal trials and J.F.B. solved the structure; K.K, D.S., C.M.R., C.H., and G.D.W. wrote the manuscript; G.D.W. supervised the project.

Notes

The authors declare no competing financial interest.

[‖]K.K., D.S., and C.M.R. contributed equally to this work.

■ ACKNOWLEDGMENTS

This work was funded by a Canadian Institutes of Health Research grant (FRN-148463), a Canadian Institutes of Health Research Fellowship award (to D.S.), an Ontario Graduate Scholarship and Queen Elizabeth II Graduate Scholarship (to C.M.R.), and a Canada Research Chair in Antibiotic Biochemistry (to G.D.W.).

■ ABBREVIATIONS

AMA- aspergillomarsmine A
L-APA- L-aminopropionic acid
L-Arg- L-arginine
L-Asn- L-asparagine
L-Asp(OtBu)- L-aspartic acid α-*t*-butyl ester
Bn- benzyl
Boc_2O- di-*tert*-butyl dicarbonate
Boc-Tyr-OH- *t*-butyloxycarbonyl tyrosine
t-Bu- *t*-butyl
CH_3CN- acetonitrile
L-Cys- L-cysteine
DCM- dichloromethane
DBU- 1,8-diazabicyclo5.4.0undec-7-ene
DIPEA- diisopropylethyl amine
DMF- dimethylformamide
DMSO- dimethyl sulfoxide
DMC-L-β,β- dimethyl-cysteine
Fmoc-Gly-OH- fluorenylmethoxycarbonyl glycine
Gly- glycine
HEPES- 2-[4-(2-hydroxyethyl)piperazin-1-yl]ethanesulfonic acid
HOBt- hydroxybenzotriazole
HBTU- 2-(1H-benzotriazole-1-yl)-1,1,3,3-tetramethyluronium hexafluorophosphate
L-His- L-histidine
IPA- isopropanol
MBL- metallo-β-lactamases
MEM- meropenem
MeOH- methanol
Me- methyl
Ns- nosyl
o-Ns-Azy-CH_2OTs- (*S*)-(1-((2-nitrophenyl) sulfonyl) aziridin-2-yl) methyl 4-methylbenzenesulfonate
o-Ns-Azi-OBn- 2-nitrophenylsulfonyl aziridin-benzyl ester
Pbf- 2,2,4,6,7-pentamethyldihydrobenzofuran-5-sulfonyl
Pen- penicillamine or DMC (dimethylcysteine)
PhSH- thiophenol
PEG- polyethylene glycol
RT- room temperature
TFA- trifluoroacetic acid
TFMSA- trifluoromethansulfomic acid
THF- tetrahydrofuran
TMTOH- trimethyltin hydroxide
Trt- trityl
Trt-D-His- $N_{(im)}$-trityl-D-histidine
Tyr- tyrosine

■ REFERENCES

(1) Ventola, C. L. The Antibiotic Resistance Crisis: Part 1: Causes and Threats. *Pharmacol. Ther.* **2015**, *40*, 277−283.

(2) King, D. T.; Sobhanifar, S.; Strynadka, N. C. J. One Ring to Rule Them All: Current Trends in Combating Bacterial Resistance to the β-Lactams. *Protein Sci.* **2016**, *25*, 787−803.

(3) Rotondo, C. M.; Wright, G. D. Inhibitors of Metallo-β-Lactamases. *Curr. Opin. Microbiol.* **2017**, *39*, 96−105.

(4) Tehrani, K. H. M. E.; Martin, N. I. B-Lactam/B-Lactamase Inhibitor Combinations: An Update. *Medchemcomm* **2018**, *9*, 1439−1456.

(5) Papp-Wallace, K. M.; Bonomo, R. A. New β-Lactamase Inhibitors in the Clinic. *Infect. Dis. Clin. North Am.* **2016**, *30*, 441−464.

(6) Kildahl-Andersen, G.; Schnaars, C.; Prandina, A.; Radix, S.; Le Borgne, M.; Jordheim, L. P.; Gjøen, T.; Andresen, A. M. S.; Lauksund, S.; Fröhlich, C.; et al. Synthesis and Biological Evaluation of Zinc Chelating Compounds as Metallo-β-Lactamase Inhibitors. *Medchemcomm* **2019**, *10*, 528−537.

(7) Shi, C.; Bao, J.; Sun, Y.; Kang, X.; Lao, X.; Zheng, H. Discovery of Baicalin as NDM-1 Inhibitor: Virtual Screening, Biological Evaluation and Molecular Simulation. *Bioorg. Chem.* **2019**, *88*, 102953.

(8) Leiris, S.; Coelho, A.; Castandet, J.; Bayet, M.; Lozano, C.; Bougnon, J.; Bousquet, J.; Everett, M.; Lemonnier, M.; Sprynski, N.; et al. SAR Studies Leading to the Identification of a Novel Series of Metallo-β-Lactamase Inhibitors for the Treatment of Carbapenem-Resistant Enterobacteriaceae Infections That Display Efficacy in an Animal Infection Model. *ACS Infect. Dis.* **2019**, *5*, 131−140.

(9) Zhang, D.; Markoulides, M. S.; Stepanovs, D.; Rydzik, A. M.; El-Hussein, A.; Bon, C.; Kamps, J. J. A. G.; Umland, K. D.; Collins, P. M.; Cahill, S. T.; et al. Structure Activity Relationship Studies on Rhodanines and Derived Enethiol Inhibitors of Metallo-β-Lactamases. *Bioorg. Med. Chem.* **2018**, *26*, 2928−2936.

(10) Danzinger, L.; Horn, K. Beta-Lactam Antibiotics. In *Drug Interactions in Infectious Diseases: Antimicrobial Drig Interactions*; Pai, M. P., Kiser, J. J., Gubbins, P. O., Rodvold, K. A., Eds.; Humana Press: Cham, 2018; pp. 1−56.

(11) Hinchliffe, P.; Moreno, D. M.; Rossi, M.-A.; Mojica, M. F.; Martinez, V.; Villamil, V.; Spellberg, B.; Drusano, G. L.; Banchio, C.; Mahler, G.; et al. 2-Mercaptomethyl Thiazolidines (MMTZs) Inhibit All Metallo-β-Lactamase Classes by Maintaining a Conserved Binding Mode. *ACS Infect. Dis.* **2021**, 2697.

(12) Ju, L. C.; Cheng, Z.; Fast, W.; Bonomo, R. A.; Crowder, M. W. The Continuing Challenge of Metallo-β-Lactamase Inhibition: Mechanism Matters. *Trends Pharmacol. Sci.* **2018**, *39*, 635−647.

(13) Tooke, C. L.; Hinchliffe, P.; Bragginton, E. C.; Colenso, C. K.; Hirvonen, V. H. A.; Takebayashi, Y.; Spencer, J. β-Lactamases and β-Lactamase Inhibitors in the 21st Century. *J. Mol. Biol.* **2019**, *431*, 3472−3500.
(14) Salari-jazi, A.; Mahnam, K.; Sadeghi, P.; Damavandi, M. S.; Faghri, J. Discovery of Potential Inhibitors against New Delhi Metallo-β-Lactamase-1 from Natural Compounds: In Silico-Based Methods. *Sci. Rep.* **2021**, *11*, 2390.
(15) Palacios, A. R.; Rossi, M. A.; Mahler, G. S.; Vila, A. J. Metallo-β-lactamase Inhibitors Inspired on Snapshots from the Catalytic Mechanism. *Biomolecules* **2020**, *10*, 854.
(16) Wade, N.; Tehrani, K. H. M. E.; Brüchle, N. C.; van Haren, M. J.; Mashayekhi, V.; Martin, N. I. Mechanistic Investigations of Metallo-β-Lactamase Inhibitors: Strong Zinc Binding Is Not Required for Potent Enzyme Inhibition. *ChemMedChem* **2021**, *16*, 1651−1659.
(17) Krajnc, A.; Brem, J.; Hinchliffe, P.; Calvopiña, K.; Panduwawala, T. D.; Lang, P. A.; Kamps, J. J. A. G.; Tyrrell, J. M.; Widlake, E.; Saward, B. G.; et al. Bicyclic Boronate VNRX-5133 Inhibits Metallo- And Serine-β-Lactamases. *J. Med. Chem.* **2019**, *62*, 8544−8556.
(18) Brem, J.; Cain, R.; Cahill, S.; McDonough, M. A.; Clifton, I. J.; Jiménez-Castellanos, J. C.; Avison, M. B.; Spencer, J.; Fishwick, C. W. G.; Schofield, C. J. Structural Basis of Metallo-β-Lactamase, Serine-β-Lactamase and Penicillin-Binding Protein Inhibition by Cyclic Boronates. *Nat. Commun.* **2016**, *7*, 12406.
(19) Lomovskaya, O.; Tsivkovski, R.; Sun, D.; Reddy, R.; Totrov, M.; Hecker, S.; Griffith, D.; Loutit, J.; Dudley, M. QPX7728, An Ultra-Broad-Spectrum B-Lactamase Inhibitor for Intravenous and Oral Therapy: Overview of Biochemical and Microbiological Characteristics. *Front Microbiol.* **2021**, *12*, 697180.
(20) Haenni, A.; Robert, M.; Vetter, W.; Roux, L.; Barbier, M.; Lederer, E. Structure Chimique Des Aspergillomarasmines A et B. *Helv. Chim. Acta* **1965**, *48*, 729−750.
(21) Sychantha, D.; Rotondo, C. M.; Tehrani, K. H. M. E.; Martin, N. I.; Wright, G. D. Aspergillomarasmine A Inhibits Metallo-β-Lactamases by Selectively Sequestering Zn2+. *J. Biol. Chem.* **2021**, *297*, 100918.
(22) King, A. M.; Reid-Yu, S. A.; Wang, W.; King, D. T.; De Pascale, G.; Strynadka, N. C.; Walsh, T. R.; Coombes, B. K.; Wright, G. D. Aspergillomarasmine A Overcomes Metallo-β-Lactamase Antibiotic Resistance. *Nature* **2014**, *510*, 503−506.
(23) Liao, D.; Yang, S.; Wang, J.; Zhang, J.; Hong, B.; Wu, F.; Lei, X. Total Synthesis and Structural Reassignment of Aspergillomarasmine A. *Angew. Chem.* **2016**, *128*, 4363−4367.
(24) Zhang, J.; Wang, S.; Wei, Q.; Guo, Q.; Bai, Y.; Yang, S.; Song, F.; Zhang, L.; Lei, X. Synthesis and Biological Evaluation of Aspergillomarasmine A Derivatives as Novel NDM-1 Inhibitor to Overcome Antibiotics Resistance. *Bioorg. Med. Chem.* **2017**, *25*, 5133−5141.
(25) Koteva, K.; King, A. M.; Capretta, A.; Wright, G. D. Total Synthesis and Activity of the Metallo-β-Lactamase Inhibitor Aspergillomarasmine A. *Angew. Chem., Int. Ed.* **2016**, *55*, 2210−2212.
(26) Albu, S. A.; Koteva, K.; King, A. M.; Al-Karmi, S.; Wright, G. D.; Capretta, A. Total Synthesis of Aspergillomarasmine A and Related Compounds: A Sulfamidate Approach Enables Exploration of Structure−Activity Relationships. *Angew. Chem., Int. Ed.* **2016**, *55*, 13259−13262.
(27) Fu, H.; Zhang, J.; Saifuddin, M.; Cruiming, G.; Tepper, P. G.; Poelarends, G. J. Chemoenzymatic Asymmetric Synthesis of the Metallo-β-Lactamase Inhibitor Aspergillomarasmine A and Related Aminocarboxylic Acids. *Nat. Catal.* **2018**, *1*, 186−191.
(28) Guo, Q.; Wu, D.; Gao, L.; Bai, Y.; Liu, Y.; Guo, N.; Du, X.; Yang, J.; Wang, X.; Lei, X.; et al. Identification of the AMA Synthase from the Aspergillomarasmine A Biosynthesis and Evaluation of Its Biocatalytic Potential. *ACS Catal.* **2020**, *10*, 6291−6298.
(29) Dortet, L.; Poirel, L.; Nordmann, P. Worldwide Dissemination of the NDM-Type Carbapenemases in Gram-Negative Bacteria. *BioMed Res. Int.* **2014**, *2014*, 249856.
(30) Khan, A. U.; Maryam, L.; Zarrilli, R. Structure, Genetics and Worldwide Spread of New Delhi Metallo-β-Lactamase (NDM): A Threat to Public Health. *BMC Microbiol.* **2017**, *17*, 101.
(31) Rotondo, C. M.; Sychantha, D.; Koteva, K.; Wright, G. D. Suppression of β-Lactam Resistance by Aspergillomarasmine A Is Influenced by Both the Metallo-β-Lactamase Target and the Antibiotic Partner. *Antimicrob. Agents Chemother.* **2020**, *64*, No. e01386-19.
(32) Zhang, J.; Wang, S.; Bai, Y.; Guo, Q.; Zhou, J.; Lei, X. Total Syntheses of Natural Metallophores Staphylopine and Aspergillomarasmine A. *J. Org. Chem.* **2017**, *82*, 13643−13648.
(33) Merrifield, R. B. Solid Phase Peptide Synthesis. *Excerpta Med., I.C.S.* **1976**, *374*, 29−39.
(34) Bonkowski, B. Basic Concepts of Using Solid Phase Synthesis to Build Small Organic Molecules Using 2-Chlorotrityl Chloride Resin. *Mod. Chem. appl.* **2013**, *01*, 2−5.
(35) Atherton, E.; Fox, H.; Harkiss, D.; Logan, C. J.; Sheppard, R. C.; Williams, B. J. A Mild Procedure for Solid Phase Peptide Synthesis: Use of Fluorenylmethoxycarbonylamino-Acids. *J. Chem. Soc., Chem. Commun.* **1978**, *13*, 537−539.
(36) Behrendt, R.; White, P.; Offer, J. Advances in Fmoc Solid-Phase Peptide Synthesis. *J. Pept. Sci.* **2016**, *22*, 4−27.
(37) Albericio, F.; El-Faham, A. Choosing the Right Coupling Reagent for Peptides: A Twenty-Five-Year Journey. *Org. Process Res. Dev.* **2018**, *22*, 760−772.
(38) FIELDS, G. B.; NOBLE, R. L. Solid Phase Peptide Synthesis Utilizing 9-fluorenylmethoxycarbonyl Amino Acids. *Int. J. Pept. Protein Res.* **1990**, *35*, 161−214.
(39) Bollhagen, R.; Schmiedberger, M.; Barlos, K.; Grell, E. A New Reagent for the Cleavage of Fully Protected Peptides Synthesised on 2-Chlorotrityl Chloride Resin. *J. Chem. Soc., Chem. Commun.* **1994**, 2559.
(40) Biron, E.; Chatterjee, J.; Kessler, H. Optimized Selective N-Methylation of Peptides on Solid Support. *J. Pept. Sci.* **2006**, *12*, 213−219.
(41) Yi, Y.; Fu, Y.; Dong, P.; Qin, W.; Liu, Y.; Liang, J.; Shang, R. Synthesis and Biological Activity Evaluation of Novel Heterocyclic Pleuromutilin Derivatives. *Molecules* **2017**, *22*, 996.
(42) Riedl, K. Studies on Pleuromutilin and Some of Its Derivatives. *J. Antibiot.* **1976**, *29*, 132−139.
(43) Jamookeeah, C. E.; Beadle, C. D.; Jackson, R. F. W.; Harrity, J. P. A. Investigation of a Flexible Enantiospecific Approach to Aziridines. *J. Org. Chem.* **2008**, *73*, 1128−1130.
(44) Nicolaou, K. C.; Estrada, A. A.; Zak, M.; Lee, S. H.; Safina, B. S. A Mild and Selective Method for the Hydrolysis of Esters with Trimethyltin Hydroxide. *Angew. Chem., Int. Ed.* **2005**, *44*, 1378−1382.
(45) Wright, G. D. Antibiotic Adjuvants: Rescuing Antibiotics from Resistance. *Trends Microbiol.* **2016**, *24*, 862−871.
(46) Richter, M. F.; Hergenrother, P. J. The Challenge of Converting Gram-Positive-Only Compounds into Broad-Spectrum Antibiotics. *Ann. N. Y. Acad. Sci.* **2019**, *1435*, 18−38.
(47) Perlmutter, S. J.; Geddes, E. J.; Drown, B. S.; Motika, S. E.; Lee, M. R.; Hergenrother, P. J. Compound Uptake into E. Coli Can Be Facilitated by N-Alkyl Guanidiniums and Pyridiniums. *ACS Infect. Dis.* **2021**, *7*, 162−173.
(48) Richter, M. F.; Drown, B. S.; Riley, A. P.; Garcia, A.; Shirai, T.; Svec, R. L.; Hergenrother, P. J. Predictive Compound Accumulation Rules Yield a Broad-Spectrum Antibiotic. *Nature* **2017**, *545*, 299−304.
(49) Neal, J. A.; Rose, N. J. Further Studies of the Coordination of Ethylenediaminedisuccinic Acid, an Isomer of Ethylenediaminetetraacetic Acid. *Inorg. Chem.* **1973**, *12*, 1226−1232.
(50) Dolomanov, O. V.; Bourhis, L. J.; Gildea, R. J.; Howard, J. A. K.; Puschmann, H. OLEX2: A Complete Structure Solution, Refinement and Analysis Program. *J. Appl. Crystallogr.* **2009**, *42*, 339−341.
(51) Sheldrick, G. M. SHELXT - Integrated Space-Group and Crystal-Structure Determination. *Acta Cryst.* **2015**, *71*, 3−8.
(52) Sheldrick, G. M. A Short History of SHELX. *Acta Cryst.* **2008**, *64*, 112−122.
(53) Zhang, Y.; Kennan, A. J. Efficient Introduction of Protected Guanidines in BOC Solid Phase Peptide Synthesis. *Org. Lett.* **2001**, *3*, 2341−2344.
(54) Kocyła, A.; Pomorski, A.; Krężel, A. Molar Absorption Coefficients and Stability Constants of Metal Complexes of 4-(2-

https://doi.org/10.1021/acsomega.1c05757
ACS Omega 2022, 7, 4170−4184

Pyridylazo)Resorcinol (PAR): Revisiting Common Chelating Probe for the Study of Metalloproteins. *J. Inorg. Biochem.* **2015**, *152*, 82−92.
(55) Hackel, M. A.; Tsuji, M.; Yamano, Y.; Echols, R.; Karlowsky, J. A.; Sahm, D. F. Reproducibility of Broth Microdilution MICs for the Novel Siderophore Cephalosporin, Cefiderocol, Determined Using Iron-Depleted Cation-Adjusted Mueller-Hinton Broth. *Diagn. Microbiol. Infect. Dis.* **2019**, *94*, 321−325.

https://doi.org/10.1021/acsomega.1c05757
ACS Omega 2022, 7, 4170−4184